The Astrophysical Journal, 699:1919–1937, 2009 July 10 doi:10.1088/0004-637X/699/2/1919

A MODEL FOR EMISSION FROM JETS IN X-RAY BINARIES: CONSEQUENCES OF A SINGLE ACCELERATION EPISODE

Asaf Pe'er[1,3] and Piergiorgio Casella[2]
[1] Space Telescope Science Institute, 3700 San Martin Dr., Baltimore, MD, 21218, USA; apeer@stsci.edu
[2] Astronomical Institute "Anton Pannekoek," University of Amsterdam, Kruislaan 403, 1098SJ, Amsterdam, Netherlands
Received 2009 February 17; accepted 2009 April 15; published 2009 June 26

ABSTRACT

There is strong evidence for powerful jets in the low/hard state of black hole X-ray binaries (BHXRBs). Here, we present a model in which electrons are accelerated once at the base of the jet, and are cooled by synchrotron emission and possible adiabatic energy losses. The accelerated electrons assume a Maxwellian distribution at low energies and possible energetic power-law tail. These assumptions yield a wealth of spectra, which we study in detail. We identify critical values of the magnetic field, and five transition frequencies in the spectra. In particular, we show that (1) for wide jets, the decay of the magnetic field along the jet enables the production of flat radio spectra without the need for electron re-acceleration along the jet; (2) an increase in the magnetic field above a critical value of $\sim 10^5$ G leads to a sharp decrease in the flux at the radio band, while the flux at higher frequencies saturates to a constant value; (3) for a strong magnetic field, the flux decays in the optical/UV band as $F_\nu \propto \nu^{-1/2}$, irrespective of the electrons' initial distribution; (4) for $B_0 \approx 10^4$ G, the X-ray flux gradually steepens; (5) with adiabatic energy losses, flat spectrum can be obtained only at a limited frequency range, and under certain conditions; and (6) for narrow jets, $r(x) \propto x^\alpha$ with $\alpha < 1/2$, flat radio spectrum cannot be obtained. We provide a full description of the spectrum in different scenarios, and show that our model is consistent with the key observed properties of BHXRBs.

Key words: plasmas – radiation mechanisms: non-thermal – stars: winds, outflows – X-rays: binaries

Online-only material: color figures

1. INTRODUCTION

Observations of the low/hard state of many black hole X-ray binaries (BHXRBs) reveal a rich broadband spectrum, extending from the radio to the hard X-rays (for reviews, see, e.g., Liang 1998; McClintock & Remillard 2006; Vrtilek 2008). Typically, the radio spectrum in the GHz–THz range is flat ($F_\nu \propto \nu^{-\alpha}$ with $\alpha \sim 0$) or slightly inverted ($\alpha < 0$) (Hynes et al. 2000; Fender 2001, 2006). This spectrum extends in some cases up to the infrared range (Chaty et al. 2003; Kalemci et al. 2005; Migliari et al. 2007). At higher energies, from the optical to the soft X-ray frequencies, the emission is dominated by a thermal irradiated disk and the companion star, while at even higher energies, hard X-rays to soft γ-rays, a power-law spectral distribution is typically observed, with a power-law index $0.5 \lesssim \alpha \lesssim 1.1$ and a variable exponential cutoff (McClintock & Remillard 2006, and references therein).

Two classes of models are often used in interpreting the nonthermal part of the X-ray spectrum: accretion-based models (e.g., Titarchuk 1994; Esin et al. 1997; Poutanen 1998; Coppi 1999; Zdziarski 2000; Esin et al. 2001) and, alternatively, jet-based models (Markoff et al. 2001, 2003, 2005; Bosch-Ramon et al. 2006; Paredes et al. 2006; Kaiser 2006). Indeed, as jets are widely believed to be the source of the observed nonthermal radio spectrum, it is possible that they also play a significant role as a source of the hard X-ray emission (see, e.g., Mirabel & Rodriguez 1999; Fender 2006). This idea had gained support by the correlation found between the observed radio and X-ray emission (Hannikainen et al. 1998; Corbel et al. 2000, 2003; Gallo et al. 2003).

A model that explains the flat radio spectra observed by the VLBI in several compact objects as due to emission from jets was suggested by Blandford & Königl (1979). In this seminal work, Blandford & Königl (1979) showed that a flat radio spectrum can naturally be obtained due to the change of the plasma conditions along the jet (in particular, the decay of the magnetic field and the decrease in the particle number density). This follows from the self-absorption of synchrotron photons, which produces a pronounced spectral break at $\nu_{\rm thick}$, the frequency below which the optical depth becomes larger than unity. The flat radio spectrum follows the dependence of this frequency on the changing plasma conditions along the jet.

In spite of their success in reproducing the observed flat radio spectra, jet models are still incomplete. In some of the models (e.g., Blandford & Königl 1979; Markoff et al. 2001, 2005; Bosch-Ramon et al. 2006) adiabatic, as well as radiative energy losses are assumed to be fully replenished by an unknown, continuous re-acceleration process along the entire jet. While re-acceleration can result from internal shocks within the jet (e.g., Kaiser et al. 2000; Spada et al. 2001; Jamil et al. 2008), there is no a priori reason to assume that it completely replenishes both the adiabatic and radiative energy losses, since the physical origin of these phenomena is different. A model developed by Hjellming & Johnston (1988) considered only adiabatic, but not radiative energy losses of the electrons. Energy losses of relativistic electrons were considered by Georganopoulos & Marscher (1998). However, this model considered only the optically thin part of the spectrum, and electron propagation close to the line of sight. A comprehensive study of jet emission which includes energy losses was carried out by Reynolds (1982), although in this work the effect of self-absorption on the electrons' energy spectrum was not considered.

A different approach was used by Kaiser (2006), who suggested a model in which only a single acceleration episode takes place, and radiation and adiabatic energy losses are not replenished. In this work, Kaiser (2006) pointed out that due to the

[3] Giacconi Fellow

decay of the magnetic field along the jet and because of self-absorption effects, flat radio spectra can naturally be obtained. Kaiser (2006) considered both conical jets in the ballistic case (i.e., neglecting adiabatic energy losses) and a scenario in which adiabatic energy losses are considered. In both cases, flat radio spectra could be obtained, albeit with specific jet geometry (a nonconical jet is required when adiabatic energy losses are considered). However, fitting the spectrum of Cyg X-1 in this model could be done only with a very narrow jet, in both the ballistic and adiabatic scenarios.

In the model by Kaiser (2006) presented above (as well as some of the former models), a power-law distribution of the accelerated electrons in the entire energy range was assumed. The break predicted in the spectrum is thus due to only the change from optically thick plasma at low energies to optically thin above $\nu_{\rm thick}$. While the details of particles' acceleration inside jets are uncertain, models of particles' acceleration in shock waves predict that the power-law distribution of electrons exists only at high energies, while a significant fraction, perhaps most, of the electrons maintain low-energy Maxwellian (thermal) distribution (Blandford & Eichler 1987; Axford 1994; Amato & Blasi 2006; Spitkovsky 2008). Thus, an inherent peak in the electron energy distribution is expected, at typical Lorentz factor $\gamma_{\rm min}$. As a result, a peak in the synchrotron spectrum is expected at frequency $\nu_{\rm peak}$ due to emission from electrons at the peak of the Maxwellian distribution. If $\nu_{\rm peak} < \nu_{\rm thick}$, then this peak is obscured; however, if $\nu_{\rm peak} > \nu_{\rm thick}$, which, as we show below, is the case for plasma parameters that are plausible for jets in black hole binaries, then two breaks in the spectrum are expected, at $\nu_{\rm thick}$ and at $\nu_{\rm peak}$.

In addition to the characteristic low-energy cutoff in the electron distribution (attributed to electrons at the peak of the Maxwellian), any physical acceleration mechanism accelerates electrons only up to a maximal Lorentz factor, denoted here by $\gamma_{\rm max}$. This introduces a maximal frequency $\nu_{\rm max}$ up to which synchrotron photons can be emitted (see, e.g., Markoff et al. 2001).

The uncertainty that exists in the nature of the acceleration process is reflected in an inherent uncertainty in the distribution of the energetic electrons. A power-law energetic tail is often assumed; however, in addition to the uncertainty in the fraction of particles that are accelerated to the energetic tail, there is an uncertainty in the spectral index of the power-law accelerated particles. Fitting data in supernovae remnants (e.g. Lazendic et al. 2004) and gamma-ray bursts (GRBs) afterglow (Galama et al. 1998; Wijers & Galama 1999; Freedman & Waxman 2001) reveal a power-law distribution with a nearly universal index, $p = 2.2 \pm 0.2$, which is consistent with theoretical expectations (Blandford & Eichler 1987). The X-ray spectra of many BHXRBs in the low/hard state show photon index that averages at $\langle\Gamma\rangle \sim 1.7$ (McClintock & Remillard 2006). If interpreted in the framework of the synchrotron emission model, this implies an electron spectral index $p \sim 2.4$, and in several cases even higher. The power-law indices inferred from fitting synchrotron emission to the X-ray spectra of BHXRBs are thus consistently higher than those obtained in other objects.

An additional inherent uncertainty in the study of emission from BHXRBs is related to the production and structure of the jet. The jet may be conical, as assumed in Blandford & Königl (1979), or confined. The jet geometry can strongly affect the radio spectra (Kaiser 2006). Another uncertainty exists in determining the microphysical processes in the jetted plasma, which governs the evolution of the magnetic field and the properties of particle acceleration to high energies, via either shock waves or other mechanisms (e.g., magnetic reconnection). The energy in the magnetic field is sometimes assumed to be in equipartition with the energy carried by the electrons (Longair 1994). However, several authors suggested the hypothesis of Poynting-flux-dominated jets (e.g., Ustyugova et al. 2000; Giannios & Spruit 2006; Komissarov et al. 2007). Indeed, in many fits (e.g., Markoff et al. 2005; Gallo et al. 2007; Migliari et al. 2007), the energy in the magnetic field is kept as a free parameter, and the fitted value is somewhat higher than equipartition value. As we show below, the value of the magnetic field affects the entire shape of the spectra in a nontrivial way.

In this paper, we combine the idea of a single acceleration episode first proposed by Kaiser (2006), with the recent results on the distribution of accelerated particles. We study here a model in which particles are accelerated only once at the base of the jet, and cool via synchrotron emission and possible adiabatic energy losses as they propagate along the jet. The magnetic field decays along the jet from its initial value at the jet base, B_0, which is taken here as a free parameter. We assume that the acceleration process produces a low-energy cutoff in the energetic electron energy distribution, in the form of a low-energy Maxwellian, accompanied by a possible energetic tail. We show that the inclusion of this inherent cutoff leads to a variety of complex spectra, which are very different than that obtained by Kaiser (2006).

This paper is organized as follows. We first introduce the basic assumptions of our model in Section 2. We solve the equations that describe the cooling rate of the energetic electrons in Section 2.3. These equations hold the key to the rest of the analysis. We discuss in Section 3 the general properties of the resulting spectra, and show that qualitatively different results are obtained for wide and narrow jets (which are defined there). We then study the resulting spectra in the different scenarios in details. In Section 4, we study the basic model of synchrotron emission (neglecting adiabatic energy losses) from a Maxwellian distribution of electrons. We extend our study in Section 5 to include a power-law distribution of energetic electrons. In Sections 6 and 7, we consider the effect of adiabatic energy losses on the obtained spectra for an initial Maxwellian and power-law distribution of the energetic electrons, respectively. We then consider in Section 8 the scenario of narrow jets. We summarize and conclude in Section 9, emphasizing the key properties of our model in view of the existing broadband data sets. Details of the numerical model that is used in producing the spectra in Figures 2–11 are given in the Appendix.

2. THE MODEL: BASIC PHYSICAL ASSUMPTIONS

Our basic jet geometry is similar to the one treated by Kaiser (2006). We consider a jet centered around the x-axis, with rotational symmetry around that axis. Denoting by x_0 the position at the base of the jet, the jet radius with respect to the x-axis at $x \geqslant x_0$ is a function of x only, $r = r(x)$. In the following, we assume a parametric dependence $r(x) = r_0(x/x_0)^{a_{\rm jet}}$. Here, r_0 is the jet radius with respect to the x-axis at x_0, and $a_{\rm jet}$ defines the jet geometry: $a_{\rm jet} = 1$ corresponds to a conical jet. Since the exact shape of BHXRB jets is not precisely known, we keep $a_{\rm jet}$ as a free parameter. In the calculation below, we assume that the observer is located at an angle $\theta^{\rm ob} \gg 0$ to the jet axis. This assumption allows us to simplify the radiative transfer calculations of synchrotron photons along the jet.

We assume that the bulk motion Lorentz factor of the plasma inside the jet is constant, and equals γ_j. This assumption can only be justified for a ballistic jet ($a_{\rm jet} = 1$). However, it was shown by Blandford & Rees (1974) that the Lorentz factor of the bulk motion of a flow in a jet is proportional to $p_x^{-1/4}$, where p_x is the pressure of the external medium that confines the jet. Assuming a shallow pressure gradient, the Lorentz factor of the flow is not expected to vary significantly along the jet. A similar argument holds for a magnetically confined jet.

The plasma in the jet originates from the accreting disk, hence its density depends on the disk accretion rate, $\dot{M}_{\rm disk}$. Following Falcke & Biermann (1995; see also Markoff et al. 2001), we assume a fraction q_j of the accreting matter to be injected into the jet. These assumptions imply that the (comoving) energy density at the base of the jet is given by $u_0 = q_j \dot{M}_{\rm disk} c^2/\pi r_0^2 \gamma_j \beta_j c$, where $\beta_j \equiv (1-\gamma_j^{-2})^{1/2}$ is the bulk motion velocity, and $r_0 \ll x_0$ is assumed.

We consider here an acceleration process that occurs entirely at x_0. This assumption is of course too simplistic. Nonetheless, we use it here in order to demonstrate the variety of spectra that can be obtained, and the spectral dependence on the uncertain value of the magnetic field, the jet geometry, and the distribution of energetic particles. Given the existing uncertainty in the nature of the acceleration process, we use two models for the accelerated electrons energy distribution, which we consider as the two extreme cases.

The first is a (relativistic) Maxwellian distribution, $n_{\rm el}(\gamma)d\gamma = A\beta\gamma^2 \exp(-\gamma/\theta_{\rm el})d\gamma$, where γ is the Lorentz factor associated with the electron random motion (not to be confused with the Lorentz factor γ_j of the bulk motion jet flow), $\beta = (1-\gamma^{-2})^{1/2}$ is their random velocity, and A is a normalization constant whose exact value is determined below. The characteristic, normalized electron temperature, $\theta_{\rm el}$, at the acceleration site $x = x_0$, is determined as follows: we assume that the plasma in the jet contains both electrons and protons. The acceleration process (e.g., a shock wave) dissipates the kinetic energy of the flow, and redistributes the proton energy between the electrons and the protons. Hence, the electrons get some fraction ϵ_e of the equipartition value of the total (electrons + protons) energy. Therefore, the average Lorentz factor associated with the electrons random motion is $\gamma_{\rm min} = \epsilon_e(m_p/m_e)$. Since in a Maxwellian energy distribution the average Lorentz factor is related to the temperature via $\gamma_{\rm min} = 3\theta_{\rm el}$, we conclude that the characteristic electron temperature at the base of the jet is

$$\theta_{\rm el}(x = x_0) \equiv \theta_{\rm el,0} = \left(\frac{\epsilon_e}{3}\right)\frac{m_p}{m_e} = 612\epsilon_{e,0}. \quad (1)$$

We adopt here and below the standard convention $Q = 10^x Q_x$ in CGS units.

Since a large number of pairs are not expected to be created, the total number density of electrons is similar to the proton number density in the plasma. At the base of the jet, it is equal to $n_{\rm el,\,tot} \approx u_0/m_p c^2$. The normalization of the accelerated electron distribution is given by $A = n_{\rm el,\,tot}/2\theta_{\rm el,0}^3$, where the factor of 2 comes from integration over the electron energy distribution: $\int_1^\infty n_{\rm el}(\gamma)d\gamma = A\theta_{\rm el,0}k_2(\theta_{\rm el,0}^{-1})$, where $k_2(\theta_{\rm el,0}^{-1}) \simeq 2\theta_{\rm el,0}^2$ is Bessel k-function of second order, and the last equality holds for $\theta_{\rm el,0} \gg 1$.

The second electron energy distribution that is considered here is a power-law distribution above $\gamma_{\rm min}$, while maintaining a Maxwellian distribution of the electron population at lower energies. This is motivated by the theoretical works discussed in Section 1. In this scenario, the power-law index of the accelerated electron energy distribution $p = -d\log n_{\rm el}(\gamma)/d\log(\gamma)$ is taken as a free parameter. The electrons are accelerated up to the maximum Lorentz factor $\gamma_{\rm max}$, whose value is determined by equating the acceleration time and the synchrotron loss time (see discussion in Section 2.1). An exponential cutoff in the electron energy distribution above $\gamma_{\rm max}$ is assumed.

The two distributions considered here rely on a strong theoretical basis and are consistent with modeling spectra from jets in GRBs (see, e.g., Pe'er & Waxman 2004). We note though that alternative acceleration models exist. For example, modeling emission from jets in blazars, Celotti & Ghisellini (2008) obtained good fits to the data with electron distribution that is consistent with power law at low energies, $\gamma_{\rm min} \gtrsim 1$.

The magnetic field evolves along the jet. We consider here a scenario in which the magnetic field is dominated by the toroidal component, $B = B_\phi \propto r^{-1}$. Therefore, $B = B_0(r/r_0)^{-1} = B_0(x/x_0)^{-a_{\rm jet}}$. The value of the magnetic field at the base of the jet, B_0, is a free parameter. One way to quantify it is by assuming that the magnetic field carries some fraction ϵ_B of the dissipated kinetic energy: $u_B = \epsilon_B u_0$, resulting in $B_0 = (8\pi\epsilon_B u_0)^{1/2}$. An equipartition value of the magnetic field is therefore obtained by setting $\epsilon_B = 1$.

As the electrons propagate along the jet at $x > x_0$, they cool via synchrotron emission and possible adiabatic energy losses. In this work, we do not consider other physical processes (such as, e.g., Compton scattering, or production of pairs). This is because of two reasons: first, for plausible parameters describing jets in BHXRBs, other phenomena are much less significant (see, e.g., Kaiser 2006). Second, the aim of this paper is to show that synchrotron emission combined with adiabatic energy losses can lead to a very large variety of possible spectra. When adiabatic energy losses are included, we use the precise formula, which is correct in the ultrarelativistic as well as the nonrelativistic regimes,

$$\frac{\partial\log(\gamma\beta)}{\partial t} = -\frac{1}{3}\frac{\partial\log(\Delta V)}{\partial t}, \quad (2)$$

which leads to $\gamma\beta \propto (\Delta V)^{-1/3}$. Here, ΔV is the volume element occupied by the particles; since the particles are assumed to propagate at a constant velocity in the x-direction, $\Delta V \propto r(x)^2$. We thus find that adiabatic energy losses result in $\gamma\beta \propto r^{-2/3}$. For energetic electrons, $\gamma \gg 1$, this formula asymptotes to the more familiar form, $\gamma \propto r^{-2/3}$.

In calculating the observed synchrotron flux, one needs to solve the radiative transfer equation along the line of sight. We use the standard assumption that the radiation field is isotropic in the comoving frame of the fluid. In this work, we limit ourselves to considering observer location at high angle to the jet propagation axis. This enables us to carry these calculations analytically. The results of the analytical approximations are then checked with the more precise numerical calculations, whose details are described in the Appendix.

We calculate the emission in the direction perpendicular to the x-axis by splitting the jet into small segments of length dx, and carrying the radiative transfer calculations at each segment independently. The surface area of a segment is $2\pi r(x)dx$. The calculation can thus be considered as a first-order approximation, although the errors are not expected to be large as long as the angle between the jet axis and the observer, $\theta^{ob} \gg 0$. In the calculation of the observed intensity below,

we further omit the Doppler factors for the approaching and receding jets, $\delta_{\mp} = [\gamma_j(1 \mp \beta_j \cos\theta^{ob})]^{-1}$. For arbitrary angle to the line of sight θ^{ob}, the Doppler factors are within the range $2\gamma_j \leqslant \delta_{\mp} \leqslant (2\gamma_j)^{-1}$ ($\delta_{\mp}[\theta^{ob} = \pi/2] = \gamma_j^{-1}$), and are therefore not much different than unity for mildly relativistic jets, $\gamma_j \gtrsim 1$.

2.1. Characteristic Frequencies of Synchrotron Emission from Electrons at the Base of the Jet

2.1.1. Maxwellian Distribution of the Accelerated Electrons

We first consider a relativistic Maxwellian energy distribution of electrons at the base of the jet, $n_{\rm el}(\gamma)d\gamma = A\beta\gamma^2 \exp(-\gamma/\theta_{\rm el,0})$, with a normalized temperature given by Equation (1). In calculating the characteristic break frequencies of the observed emission in our model, we use the same parameter values that were used by Markoff et al. (2001) in fitting the broadband spectrum of XTE J1118+480. This gives possible values of the free model parameters that can be used for illustrative purposes.

We therefore assume a disk accretion rate $\dot{M}_{\rm disk} = 3 \times 10^{-8}\, M_\odot\, {\rm yr}^{-1}$ around a $M_{\rm BH} = 6\, M_\odot$ black hole, an efficiency in matter injection into the jet $q_j = 10^{-2}$, and bulk motion Lorentz factor of the matter inside the jet $\gamma_j = 2$. We take the jet base to be at a distance $x_0 = 45 r_s$ from the black hole, and the jet radius at its base to be $r_0 = 10 r_s$, where r_s is the Schwarzschild radius. With these assumptions, the energy density at the base of the jet is

$$u_0 = \frac{q_j \dot{M}_{\rm disk} c}{\pi r_0^2 \gamma_j \beta_j} = \frac{10^{26}}{r_0^2}\bar{u}_0 \ {\rm erg\,cm^{-3}}, \quad (3)$$

where $\bar{u}_0 = q_{j,-2}(\dot{M}_{\rm disk}/10^{7.5} M_\odot\, {\rm yr}^{-1})(\gamma_j/2)$ is a dimensionless quantity, whose value depends on the flow parameters. For the nominal values taken here, the normalization of the electron distribution, $A_0 \equiv A(x = x_0) = 5 \times 10^5\ \bar{u}_0\, r_{0,1}^{-2}\, \epsilon_{e,0}^{-3}\, {\rm cm}^{-3}$, and the magnetic field at the base of the jet, $B_0 = 9 \times 10^4\, \bar{u}_0^{1/2}\, r_{0,1}^{-1}\, \epsilon_{B,-3}^{1/2}$ G, are readily determined. Here, $r_{0,1} = r_0/10 r_s$.

The peak frequency of the spectrum is determined by synchrotron emission from electrons at the peak of the Maxwellian. At the base of the jet,

$$\nu_{\rm peak,0} \equiv \nu_{\rm peak}(x = x_0) = \frac{3\theta_{\rm el,0}^2}{4\pi}\frac{q B_0}{m_e c} \simeq 1.4 \times 10^{17}\, \bar{u}_0^{1/2}\, r_{0,1}^{-1}\, \epsilon_{e,0}^2\, \epsilon_{B,-3}^{1/2}\ {\rm Hz}. \quad (4)$$

Synchrotron emissivity from a Maxwellian distribution of electrons was calculated by Jones & Hardee (1979). For $z \equiv 3\nu/2\nu_{\rm peak} \lesssim 1$, it was found that $j_\nu(z \lesssim 1) = (4/9)(A\theta_{\rm el}^3 q^3 B_0/m_e c^2)(z/2)^{1/3}$, while for $z \gg 1$ the flux decays exponentially, $j_\nu(z \gg 1) = (\pi/4)(A\theta_{\rm el}^3 q^3 B_0 z/m_e c^2) \exp[-(3/2)(2z)^{1/3}]$.

For a propagation direction perpendicular to the x-axis, the photons travel distance $r(x)$ before escaping the jet. The optical depth to synchrotron self-absorption of these photons is given by (e.g., Rybicki & Lightman 1979)

$$\tau_\nu = \frac{j_\nu c^2 r(x)}{2\nu^2 m_e c^2 \theta_{\rm el}}. \quad (5)$$

The break frequency is defined as the frequency below which the optical depth is larger than unity, $\nu_{\rm thick} = \nu|_{\tau_\nu = 1}$. Taking $\nu_{\rm thick} < \nu_{\rm peak}$ (i.e., $z < 1$) at the jet base, using Equations (4) and (5), one finds that at the base of the jet

$$\nu_{\rm thick,0} \equiv \nu_{\rm thick}(x = x_0) = \left(\frac{2}{9}\frac{A\theta_{\rm el,0}^2 q^3 B_0 r_0}{m_e^2 c^2}\right)^{3/5}\left(\frac{3}{4\nu_{\rm peak,0}}\right)^{1/5} = \left(\frac{8\pi^2}{9^3}\frac{u_0^4 q^8 r_0^3 \epsilon_B}{m_e^5 m_p^3 c^{11}}\right)^{1/5}\frac{1}{\theta_{\rm el,0}} \simeq 2.1 \times 10^{13}\ \bar{u}_0^{4/5} \times r_{0,1}^{-1}\, \epsilon_{e,0}^{-1}\, \epsilon_{B,-3}^{1/5}\ {\rm Hz}. \quad (6)$$

The condition $\nu_{\rm peak,0} \geqslant \nu_{\rm thick,0}$ can thus be written as a requirement on the energy carried by the electrons,

$$\epsilon_{e,0} \geqslant 5.3 \times 10^{-2}\ \bar{u}_0^{1/10}\, \epsilon_{B,-3}^{-1/10}. \quad (7)$$

The weak dependence on the parameters of the flow and on the magnetic field implies that for a wide range of parameters, the right-hand side of Equation (7) is smaller than unity. Thus, for near equipartition value of the energy carried by the electrons $\epsilon_{e,0} \lesssim 1$, the peak emission frequency at the jet base is above the break frequency.

2.1.2. Power-law Distribution of the Accelerated Electrons

Our second acceleration scenario considers a power-law distribution of the energetic electrons above the peak of the Maxwellian: $n_{\rm el}(\gamma)d\gamma \propto \gamma^{-p}$ for $\gamma_{\rm min} < \gamma < \gamma_{\rm max}$. The power-law index p of the electron energy distribution is taken as a free parameter. We estimate the maximum Lorentz factor of the accelerated electrons by equating the acceleration time, $t_{\rm acc} \simeq E/cqB_0$, with the synchrotron cooling time, $9m_e^3c^5/4q^4B_0^2\gamma$, to obtain $\gamma_{\rm max} = (3/2)m_e c^2/(q^3 B_0)^{1/2}$. Synchrotron emission from these electrons is expected at

$$\nu_{\rm max,0} = \frac{3}{4\pi}\frac{\gamma_{\rm max}^2 q B_0}{m_e c} = \frac{27}{16\pi}\frac{m_e c^3}{q^2} = 5.7 \times 10^{22}\ {\rm Hz}. \quad (8)$$

Note that this value is independent of the strength of the magnetic field at the acceleration site.

The minimum Lorentz factor of the power-law distribution, $\gamma_{\rm min}$, is determined self-consistently once the power-law index p, the maximum Lorentz factor $\gamma_{\rm max}$, and the total number and energy densities of the accelerated electrons are known (see further explanation on the numerical model in the Appendix). Below $\gamma_{\rm min}$, a Maxwellian distribution is assumed, with temperature $\theta_{\rm el,0} = \gamma_{\rm min}/2$, chosen such that the low-energy Maxwellian smoothly connects to the power-law distribution at higher energies. The inclusion of a low-energy Maxwellian distribution implies that the results derived above in Equations (4)–(7) hold in this scenario as well.

2.2. Observed Flux from a Jet Segment

For an observer located at high angle to the x-axis, a jet segment has a surface area $2\pi r(x)dx$. The flux observed from a jet segment of length dx is thus

$$dF_\nu = \frac{r(x)^2}{2d^2}\frac{j_\nu}{\tau_\nu}(1 - e^{-\tau_\nu})dx, \quad (9)$$

where d is the distance, and we omitted the dependence on the Doppler factors.

For a Maxwellian distribution of electrons, the observed spectrum from a jet segment can therefore be described by

a broken power law with two characteristic frequencies: for $\nu \ll \nu_{\rm thick}$, $\tau_\nu \gg 1$, and

$$dF_\nu(\nu \ll \nu_{\rm thick}) \simeq \frac{r(x)^2}{2d^2}\frac{j_\nu}{\tau_\nu}dx = \frac{r(x)}{d^2} m_e \theta_{\rm el} \nu^2 dx, \quad (10)$$

is proportional to ν^2. For $\nu_{\rm thick} \lesssim \nu \lesssim \nu_{\rm peak}$, the optical depth $\tau_\nu \lesssim 1$, and

$$dF_\nu(\nu_{\rm thick} \lesssim \nu \lesssim \nu_{\rm peak}) \simeq \frac{r(x)^2}{2d^2} j_\nu dx = \frac{2r(x)^2}{9d^2}\frac{A\theta_{\rm el}^3 q^3 B}{m_e c^2}\left(\frac{3\nu}{4\nu_{\rm peak}}\right)^{1/3} dx, \quad (11)$$

is proportional to $\nu^{1/3}$. For $\nu \gtrsim \nu_{\rm peak}$, the emissivity j_ν decays exponentially, and therefore an exponential cutoff in the observed flux is expected.

In this work, we focus on a scenario in which ϵ_e is close to equipartition. However, we note that if the electrons carry a much smaller fraction of the energy such that the condition in Equation (7) is not fulfilled, then $\nu_{\rm thick,0} > \nu_{\rm peak,0}$. Moreover, even if $\epsilon_e \simeq 1$, as we will show below, both $\nu_{\rm peak}$ and $\nu_{\rm thick}$ can vary along the jet in different ways. As a result, there exists a transition radius $x_{\rm trans}$ above which $\nu_{\rm thick}(x > x_{\rm trans}) > \nu_{\rm peak}(x > x_{\rm trans})$. Once this occurs, the emission from a jet segment is composed of a thick part below $\nu_{\rm thick}$ where $dF_\nu \propto \nu^2$, and an exponential cutoff at higher frequencies.

When a power-law distribution of electrons is considered, in order to calculate the emissivity and flux, one needs to specify the fraction of electrons that are accelerated to the high-energy tail above the Maxwellian. For demonstration purposes, we consider here complete acceleration to the energetic tail, while maintaining the low-energy Maxwellian and high-energy cutoff in the distribution. Thus, the power-law distribution smoothly connects to the peak of the Maxwellian. In this case, calculation of the frequency dependence of the flux in Equations (9)–(11) holds (though a slight modification exists in the overall normalization of the flux).

We can thus conclude that there are two main differences in the emissivity from a jet segment in a power-law scenario and the pure Maxwellian distribution considered above. The first difference is that standard calculations (e.g., Rybicki & Lightman 1979) show that above $\nu_{\rm peak}$ (and below $\nu_{\rm max}$) there is a power-law decrease of the flux, with power-law index $(p-1)/2$. An exponential cutoff exists only above $\nu_{\rm max}$, while in a pure Maxwellian distribution an exponential cutoff exists already above $\nu_{\rm peak}$.

The second difference is relevant if $\nu_{\rm thick}(x) > \nu_{\rm peak}(x)$. For a power-law distribution of electrons, the thick part of the spectrum ($\nu < \nu_{\rm thick}$) is characterized by $F_\nu \propto \nu^{5/2}$ (e.g., Rybicki & Lightman 1979), while a power-law $F_\nu \propto \nu^{(p-1)/2}$ is kept above $\nu_{\rm thick}$. Here, however, we expect a somewhat more complex spectral shape at low frequencies $\nu < \nu_{\rm thick}$: for $\nu \lesssim \nu_{\rm thick}$, $F_\nu \propto \nu^{5/2}$, while at much lower frequencies, the flux is $F_\nu \propto \nu^2$ due to the inclusion of a low-energy Maxwellian.

2.3. Electron Energy Loss Along the Jet

As the electrons propagate along the jet, they cool by synchrotron emission, as well as possible adiabatic energy losses. As a result, the characteristic frequencies derived above for $x = x_0$ vary along the jet. We calculate in this section the change in the electron energy distribution due to synchrotron and adiabatic cooling.

As they propagate along the jet, the electrons cool via synchrotron emission, and their momentum decreases at a rate $d(\gamma\beta)/dt|_{\rm sync} = -(4/3)c\sigma_T/(m_e c^2) u_B (\gamma\beta)^2$. Here, σ_T is Thomson's cross section and $u_B = B^2/8\pi$ is the energy density in the magnetic field. Along the jet, the magnetic field decays as $B(x) = B_0(x/x_0)^{-a_{\rm jet}}$. Since the bulk velocity of the electron propagation is taken to be constant, the electron position along the jet (x)-axis is related to the (comoving) time they spend in the jet by $x = \gamma_j\beta_j ct$; thus, the electrons reach the acceleration site (at the base of the jet) at time $t_0 = x_0/\gamma_j\beta_j c$.

Adiabatic energy losses (see Equation (2)) are quantified by $d(\gamma\beta)/dt|_{\rm ad} = -(2/3)(a_{\rm jet}/t)\gamma\beta$. Considering both synchrotron and adiabatic energy losses, the electron momentum decay (in the bulk motion comoving frame) is governed by (Longair 1994; Kaiser 2006)

$$\frac{d(\gamma\beta)}{dt} = -\frac{4\sigma_T}{3m_e c}\frac{B_0^2}{8\pi}\left(\frac{t}{t_0}\right)^{-2a_{\rm jet}}(\gamma\beta)^2 - \frac{2a_{\rm jet}}{3t}(\gamma\beta). \quad (12)$$

The solution to Equation (12) was derived by Kaiser (2006),

$$\gamma\beta(t) = \frac{\gamma\beta(t_0)\times(t/t_0)^{-2a_{\rm jet}/3}}{1+\frac{\sigma_T B_0^2 t_0}{6\pi m_e c(8a_{\rm jet}/3-1)}\gamma\beta(t_0)[1-(t/t_0)^{1-8a_{\rm jet}/3}]}. \quad (13)$$

If adiabatic energy losses are neglected, then the second term on the right-hand side of Equation (12) is dropped, and the solution is

$$\gamma\beta(t) = \frac{\gamma\beta(t_0)}{1+\frac{\sigma_T B_0^2 t_0}{6\pi m_e c(2a_{\rm jet}-1)}\gamma\beta(t_0)[1-(t/t_0)^{1-2a_{\rm jet}}]}. \quad (14)$$

Equation (14) reveals an important result, which was first derived by Kaiser (2006): if adiabatic energy losses are not included, for $a_{\rm jet} > 1/2$, the Lorentz factor of the electrons asymptotes at $t \to \infty$ to a value larger than unity. This implies that some part of the electron initial energy is maintained and not radiated. The origin of this counterintuitive result is the decay of the magnetic field along the jet. It provides a natural, possible mechanism for maintaining the electron (asymptote) temperature, as is required by, e.g., the model of Blandford & Königl (1979), without the need for particle re-acceleration along the jet. This fact also allows us to define wide jets in this case as jets for which $a_{\rm jet} > 1/2$.

We present in Figure 1 several examples of the electron momentum temporal decay due to synchrotron and adiabatic energy losses (Equation (13)) and pure synchrotron cooling (Equation (14)). In producing the results, we consider a conical jet ($a_{\rm jet} = 1$), and four different values of the magnetic field, $B_0 = 10^4$, $10^{4.5}$, 10^5, and $10^{5.5}$ G. An additional plot illustrates the scenario of a narrow jet ($a_{\rm jet} = 0.1$) and $B_0 = 10^{4.5}$ G. Asymptotic behavior of the electron momentum at late times, $t \gg t_0$, is clearly seen (and easily derived from Equations (13) and (14)). When adiabatic energy losses are considered, for wide jets, $a_{\rm jet} > 3/8$, the electron momentum decays asymptotically as $\gamma\beta \propto t^{-2a_{\rm jet}/3}$. For pure synchrotron cooling and $a_{\rm jet} > 1/2$, the electron momentum reaches a constant value. Interestingly, we find from Equations (13) and (14) that in narrow jets, $a_{\rm jet} < 3/8$, the electrons' asymptotic decay law is similar in both scenarios, i.e., independent of the inclusion of adiabatic

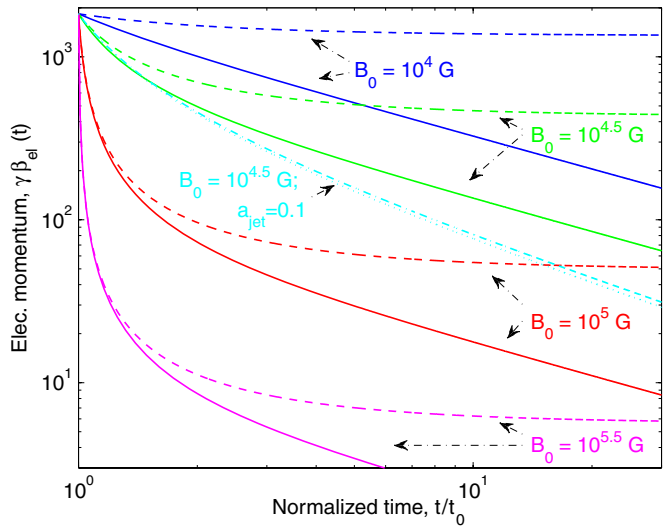

Figure 1. Temporal decay of the electron momentum, $\gamma\beta(t)$, as a function of time. Shown are adiabatic + synchrotron (solid lines, Equation (13)) and pure synchrotron (dashed lines, Equation (14)) scenarios. Four values of the magnetic field are considered (from top to button), $B_0 = 10^4, 10^{4.5}, 10^5, 10^{5.5}$ G. The dotted lines (light blue) show the decay of the electrons' energy for a narrow jet, $a_{\rm jet} = 0.1$ and $B_0 = 10^{4.5}$ G. In all the other cases, we consider a conical jet ($a_{\rm jet} = 1$). The values of the flow parameters used in determining t_0 are the same as those used in Section 2.1.1, resulting in $t_0 = x_0/\gamma_j\beta_j c = 1.5 \times 10^{-3}$ s, and an initial electron momentum $\gamma\beta_{\rm el}(t_0) = m_p/m_e = 1836$. For pure synchrotron and $a_{\rm jet} > 1/2$, the momentum asymptotes at $t \gg t_0$ to a finite value, while for synchrotron and adiabatic losses, at $t \gg t_0$, $\gamma\beta(t) \propto t^{-2a_{\rm jet}/3}$. An important result is that the initial rapid decay occurs on a timescale $t/t_0 \lesssim$ few. See the text for details.

(A color version of this figure is available in the online journal.)

energy losses. In this case, for $t \gg t_0$, both scenarios result in electron momentum asymptotic decay law $\gamma\beta \propto t^{2a_{\rm jet}-1}$.

For a strong value of the magnetic field, the asymptotic behavior of the electron momentum is reached after a very rapid decay of the electron initial energy, or momentum. This rapid decay results from an extensive synchrotron emission in the strong magnetic field close to the jet base. The results presented in Figure 1 illustrate an important point that will be extensively used in the analysis in the following sections: in a strong magnetic field, the initial rapid decay in the electron momentum takes place on a very short timescale, $t/t_0 \lesssim$ few, which is translated to a very short spatial scale—the rapid cooling (and most of the radiation) occurs very close to the jet base.

This enables us to obtain an analytical approximation to the observed flux by splitting the jet into two separated regimes. We first calculate the emissivity during the rapid cooling phase, which takes place close to the jet base, hence the magnetic field can be approximated as constant during this phase. At a second step, we calculate the emissivity during the rest of the electrons' propagation along the jet, assuming that the electron temperature evolution follows its asymptotic behavior. The approximate analytical results are compared with the exact results obtained numerically.

3. GENERAL PROPERTIES OF THE SPECTRA

As we will show in Sections 4–8, a wealth of spectra can be obtained, whose details depend on the various model assumptions. In particular, we will show that the observed spectra are very sensitive to the strength of the magnetic field. This dependence is found to be highly nontrivial. In addition, both the jet geometry and the initial particle distribution significantly affect the obtained spectrum. Therefore, before discussing the various possibilities in detail, we first discuss in this section some general properties of the emission along the jet. Here, we focus on global properties of the observed spectra, which are direct consequences of our models' assumptions as stated in Section 2. The detailed spectra expected in the various scenarios will be discussed in the following sections.

3.1. Critical Values of the Magnetic Field at the Base of the Jet

We showed in Section 2.3 that for a strong magnetic field at the jet base, the electron temporal behavior can be separated roughly into two distinctive regimes (see Figure 1). At the first stage, the electrons rapidly cool due to synchrotron emission. This stage lasts a very short duration, of the order $t/t_0 \lesssim$ few. Following the rapid energy loss, at a second stage the electron cooling rate asymptotes to its terminal value. If only synchrotron emission is considered and $a_{\rm jet} > 1/2$, then the electrons maintain their energy, and their Lorentz factor, or momentum, becomes time independent, $\gamma\beta(t) \propto t^0$ at $t \gg t_0$. If adiabatic energy losses are considered, then for $a_{\rm jet} > 3/8$ the electron momentum decays at late times $t \gg t_0$ in accordance with $\gamma\beta(t) \propto t^{-2a_{\rm jet}/3}$. For lower values of $a_{\rm jet}$, both scenarios yield a similar result, $\gamma\beta(t) \propto t^{2a_{\rm jet}-1}$.

The fact that the rapid decay phase exists only very close to the jet base, in regions where the magnetic field is approximately constant (and equals B_0), combined with the fact that the accelerated electron distribution has characteristic energies, enables one to define critical values for the strength of the magnetic field at the jet base. As we will show below, these critical values represent qualitative transitions in the resulting spectra. The critical values are defined as follows.

If the acceleration process produces a Maxwellian energy distribution, then the energetic electrons have a characteristic Lorentz factor, $\gamma_{\rm min}(t_0) = 3\theta_{\rm el,0}$. Due to the exponential decay nature of this distribution at high energies, there are effectively no electrons with Lorentz factor $\gamma \gg \gamma_{\rm min}$. The cooling rate depends both on the electrons' energy, or momentum, and on the strength of the magnetic field at the jet base, B_0 (see Equations (12)–(14)). One can therefore conclude that for very weak magnetic field, the rapid decay phase is insignificant and the entire electron distribution is effectively unchanged during this phase. This case is illustrated in Figure 1, for $B_0 = 10^4$ G. If, on the other hand, the magnetic field is stronger than a certain value, the initial electron cooling is significant.

This fact allows us to define a critical value of the magnetic field at the jet base, as a value above which electrons at the peak of the Maxwellian distribution significantly lose their energy by synchrotron emission during the initial rapid cooling phase. For the pure synchrotron case (neglecting adiabatic energy losses) and wide jets ($a_{\rm jet} > 1/2$), this critical value is formally obtained by taking the limit $t \gg t_0$ in Equation (14), and equating the second term in the denominator with unity,

$$B_{\rm cr,1} = 1.6 \times 10^4\,(2a_{\rm jet}-1)^{1/2}\,\epsilon_{e,0}^{-1/2}(\gamma_j/2)^{1/2}(x_0/45r_s)^{-1/2}\ {\rm G},$$
$$\epsilon_{B,{\rm cr},1} = 3 \times 10^{-5}\,(2a_{\rm jet}-1)\,\epsilon_{e,0}^{-1}\,(\gamma_j/2)\,\bar{u}_0^{-1}\,r_{0,1}^2\,(x_0/45r_s)^{-1}. \quad (15)$$

While the results in Equation (15) are formally derived for the pure synchrotron scenario in wide jets, one finds that the timescale of the initial, rapid cooling is similar when adiabatic energy losses are included (see Equations (13) and

(14), and Figure 1) and in the case of narrow jets. Therefore, the results derived in Equation (15) also hold in these cases (mathematically, the only difference is to replace the factor $2a_{\rm jet}-1$ with a similar factor $8a_{\rm jet}/3-1$ when adiabatic energy losses are added). We can therefore summarize that for $B_0 < B_{\rm cr,1}$, the initial rapid cooling is insignificant.

Our second acceleration model considers a power-law energy distribution of the accelerated electrons above the peak of the Maxwellian and below a maximum Lorentz factor $\gamma_{\rm max}$. Equations (13) and (14) that describe the decay of the electron Lorentz factor due to synchrotron emission and adiabatic cooling are independent of the electron distribution, and hence are valid in this scenario as well.

The inclusion of a maximum Lorentz factor of the electron energy distribution $\gamma_{\rm max}$ implies that one can define an additional critical value of the magnetic field, $B_{\rm cr,0}$, in a similar way to the definition of $B_{\rm cr,1}$. It is defined as the value of the magnetic field below which electrons at $\gamma_{\rm max}$ do not cool significantly by synchrotron emission. Repeating the analysis carried out above shows that

$$B_{\rm cr,0} = 270\,(2a_{\rm jet}-1)^{2/3}\,(\gamma_j/2)^{2/3}\,(x_0/45r_s)^{-2/3}\ {\rm G},$$
$$\epsilon_{B,{\rm cr},0} = 10^{-8}\,(2a_{\rm jet}-1)^{4/3}\,(\gamma_j/2)^{4/3}\,(x_0/45r_s)^{-4/3}\bar{u}_0^{-1}\,r_{0,1}^2. \quad (16)$$

We thus conclude that for very low values of the magnetic field, $B_0 < B_{\rm cr,0}$, the distribution of the power-law-accelerated electrons in the entire energy range is unaffected by the initial rapid cooling phase. If the magnetic field is stronger, $B_{\rm cr,0} < B_0 < B_{\rm cr,1}$, then the highest end of the electron distribution is cooled rapidly close to the jet base, while for electrons at the low end of the distribution, with $\gamma \gtrsim \gamma_{\rm min}$, the initial cooling is inefficient. As a result, the main effect of the initial rapid cooling is a shift of the highest energy tail in the electron energy distribution to lower energies. This result affects the observed spectrum at high energies, and will be discussed in Section 5.

For higher values of the magnetic field, the initial rapid cooling of the energetic electrons is significant. In the pure synchrotron case and $a_{\rm jet} > 1/2$, following the initial rapid decay, the electron Lorentz factor asymptotes to a constant value. Since in this case at $t \gg t_0$ the second term in the denominators of both Equations (13) and (14) is larger than unity, one finds a simple analytical expression for the energetic electrons' asymptotic momentum,

$$(\gamma\beta)_f = \gamma\beta(t \gg t_0) \simeq \frac{6\pi m_e c(2a_{\rm jet}-1)}{\sigma_T B_0^2 t_0}. \quad (17)$$

The electron Lorentz factor at the end of the rapid cooling phase is therefore independent of its initial Lorentz factor, and is inversely proportional to B_0^2 (see Figure 1). Similar to the discussion that followed Equation (15), we point out that while Equation (17) was derived for the pure synchrotron case, a similar equation holds when adiabatic losses are included.

If the magnetic field is in the range $B_{\rm cr,0} < B_0 < B_{\rm cr,1}$, then the rapid cooling affects only electrons at the high end of the power-law energy distribution, while if the initial distribution is a Maxwellian, the entire electron distribution is unchanged. For stronger value of the magnetic field, $B_0 > B_{\rm cr,1}$, electrons at and above the peak of the Maxwellian rapidly cool. Since the electron Lorentz factor at the end of the rapid cooling γ_f is independent of its initial Lorentz factor, in both the Maxwellian and power-law acceleration scenarios we expect a quasi-Maxwellian distribution to be formed at the end of the initial rapid cooling phase (see the numerical results in the figures below). This quasi-Maxwellian distribution is characterized by temperature $\theta_{{\rm el},f} = \gamma_f/3$.

During the initial rapid decay phase, the magnetic field is nearly constant. However, the characteristic frequencies $\nu_{\rm peak}$ and $\nu_{\rm thick}$ depend on the electron temperature, and therefore vary as the electrons cool (see Equations (4) and (6)). While the peak frequency $\nu_{\rm peak}$ decreases when the electrons lose their energy, the break frequency $\nu_{\rm thick}$ increases. Therefore, if the electrons cool to below a critical temperature,

$$\theta_{\rm cr} = \left(\frac{4}{3}\right)^{1/3}\left(\frac{\pi^2 u_0 q r_0}{9B_0 m_p c^2}\right)^{1/5} = 30\,\bar{u}_0^{1/10}\epsilon_{B,-3}^{-1/10}, \quad (18)$$

then at the end of the rapid cooling phase, $\nu_{{\rm thick},f} \equiv \nu_{\rm thick}(x = x_0; \theta_{\rm el} = \theta_{{\rm el},f}) \geqslant \nu_{{\rm peak},f}$. The condition that the electrons cool to temperature $\theta_{{\rm el},f} \leqslant \theta_{\rm cr}$ can be phrased as a condition on the strength of the magnetic field at the base of the jet. Using Equation (17), one finds that this happens for $B_0 \geqslant B_{\rm cr,2}$, where

$$B_{\rm cr,2} = 8.0\times10^4\,(2a_{\rm jet}-1)^{5/9}\,(\gamma_j/2)^{5/9} \times (x_0/45r_s)^{-5/9}\,\bar{u}_0^{-1/9}\,r_{0,1}^{1/9}\ {\rm G},$$
$$\epsilon_{B,{\rm cr},2} = 8.0\times10^{-4}\,(2a_{\rm jet}-1)^{10/9}\,(\gamma_j/2)^{10/9} \times (x_0/45r_s)^{-10/9}\,\bar{u}_0^{-11/9}\,r_{0,1}^{20/9}. \quad (19)$$

We thus conclude that if the magnetic field is intermediate, $B_{\rm cr,1} < B_0 < B_{\rm cr,2}$, then at the end of the initial cooling phase, still the peak of the emission is in the optically thin region, $\nu_{{\rm peak},f} \geqslant \nu_{{\rm thick},f}$. For higher values of the magnetic field, at the end of the rapid cooling phase, the peak of the emission is obscured, $\nu_{{\rm thick},f} \geqslant \nu_{{\rm peak},f}$.

3.2. Asymptotic Variations of the Characteristic Frequencies Along the Jet and the Transition Frequency

The change in the electron energy distribution and the decay of the magnetic field along the jet imply that the characteristic emission frequencies, $\nu_{\rm thick}$ and $\nu_{\rm peak}$, vary along the jet. Equations (13) and (14) give the decay laws of the electrons energy along the jet, and thus enable us to calculate the variation of these frequencies. Although these equations show complex dependence of the electrons' energy in time, the discussions in Sections 2.3 and 3.1 show that following an initial rapid decay phase, the electrons decay laws at times $t \gtrsim t_0$ asymptotes to simple, analytical functions of time. Therefore, the temporal dependence of the characteristic frequencies can also be described analytically in this limit.

If adiabatic energy losses are ignored, then for $a_{\rm jet} > 1/2$ the electron temperature asymptotes to a constant, finite value. Thus, we consider the asymptotic temporal dependence $\theta_{\rm el} \propto t^0 \propto r^0$. In this case, the electron number and energy densities drop as $n_{{\rm el,\,tot}}(r) \propto r^{-2}$, $u(r) \propto r^{-2}$, resulting in a decay of the proportionality constant $A(r) \propto r^{-2}$. Since the magnetic field also decays as $B(r) \propto r^{-1}$, one finds from Equations (4) and (6) that the characteristic frequencies decay in a similar way,

$$\nu_{\rm peak} \propto \nu_{\rm thick} \propto r^{-1} \propto x^{-a_{\rm jet}}. \quad (20)$$

When adiabatic energy losses are considered, for $a_{\rm jet} > 3/8$, at $t \gtrsim t_0$, the electron temperature decays as $\theta_{\rm el}(t) \propto t^{-2a_{\rm jet}/3} \propto r^{-2/3}$. The electron number density drops as $n_{{\rm el,\,tot}}(r) \propto r^{-2}$, and

therefore the electron energy density decays as $u(r) \propto r^{-8/3}$. As a result, the characteristic frequencies decay according to

$$\nu_{\rm peak} \propto B\theta_{\rm el}^2 \propto r^{-7/3} \propto x^{-7a_{\rm jet}/3}$$
$$\nu_{\rm thick} \propto (u^3 B^2 r^3)^{1/5} \theta_{\rm el}^{-1} \propto r^{-11/15} \simeq x^{-2a_{\rm jet}/3}. \quad (21)$$

The different x-dependent of the two frequencies implies that when adiabatic energy losses are considered, even if at the base of the jet $\nu_{\rm peak,0} > \nu_{\rm thick,0}$, then far enough along the jet, at $x > x_{\rm trans}$, $\nu_{\rm thick}(x) > \nu_{\rm peak}(x)$. In order to estimate the transition distance $x_{\rm trans}$, we discriminate between two cases.

1. $B_0 < B_{\rm cr,1}$. In a weak magnetic field, the electrons do not undergo the initial rapid cooling phase, and one finds that $x_{\rm trans}/x_0 = (\nu_{\rm peak,0}/\nu_{\rm thick,0})^{5/8a_{\rm jet}}$, or

$$\frac{x_{\rm trans}}{x_0} = (250)^{1/a_{\rm jet}}\, \bar{u}_0^{-3/(16a_{\rm jet})}\, \epsilon_{e,0}^{15/(8a_{\rm jet})}\, \epsilon_{B,-3}^{3/(16a_{\rm jet})}. \quad (22)$$

At $x_{\rm trans}$, $\nu_{\rm thick}(x_{\rm trans}) = \nu_{\rm peak}(x_{\rm trans})$, and both are equal to

$$\nu_{\rm trans}(B_0 < B_{\rm cr,1}) = 3.7 \times 10^{11}\, \bar{u}_0^{15/16}\, r_{0,1}^{-1}\, \epsilon_{e,0}^{-19/8}\, \epsilon_{B,-3}^{1/16}\ {\rm Hz}. \quad (23)$$

Thus, a change in the spectrum at $\nu_{\rm trans}$ is expected.

2. $B_{\rm cr,1} < B_0$. In this case the electrons rapidly cool before their temperature asymptotes. Thus, at the end of the rapid cooling, the ratio between the peak and break frequencies is $\nu_{{\rm peak},f}/\nu_{{\rm thick},f} = \nu_{\rm peak,0}/\nu_{\rm thick,0} \times (\theta_{{\rm el},f}/\theta_{\rm el,0})^3$. Following the initial rapid cooling, the asymptotic behavior of the two frequencies follows a similar decay law to the one considered above in Equation (21), and therefore one finds that the transition from optically thick to optically thin emission occurs at frequency

$$\nu_{\rm trans}(B_{\rm cr,2} > B_0 > B_{\rm cr,1}) = 1.1 \times 10^{15}\, (8a_{\rm jet}/3 - 1)^{-19/8} \times \bar{u}_0^{53/16} r_{0,1}^{-23/4}\, (\gamma_j/2)^{-19/8} \times (x_0/45r_s)^{19/8}\, \epsilon_{B,-3}^{39/16}\ {\rm Hz}. \quad (24)$$

By definition, if $B_0 > B_{\rm cr,2}$ then the transition to the optically thick emission occurs already at the base of the jet.

For narrow jets, $a_{\rm jet} < 1/2$, the electron temperature decays as $\theta_{\rm el} \propto x^{2a_{\rm jet}-1}$, and their energy density drops as $u \propto x^{-1}$. As a result, the peak frequency decays as $\nu_{\rm peak}(x) \propto x^{3a_{\rm jet}-2}$, while the break frequency as $\nu_{\rm thick} \propto x^{(-9a_{\rm jet}+2)/5}$. We find that the transition frequency depends on the jet geometry in a complex way:

$$\nu_{\rm trans}(a_{\rm jet} < 1/2) \approx 10^{17} \times (7 \times 10^3)^{A_1}\, \bar{u}_0^{1/2-3A_2/10} \times r_{0,1}^{-1}\, \epsilon_{e,0}^{2+3A_2}\, \epsilon_{B,-3}^{1/2+3A_2/10}\ {\rm Hz}, \quad (25)$$

where $A_1(a_{\rm jet}) = (15a_{\rm jet} - 10)/(12 - 24a_{\rm jet})$, and $A_2(a_{\rm jet}) = (12 - 24a_{\rm jet})(3a_{\rm jet} - 2)/5$. The transition frequency varies as a power in $A_1(a_{\rm jet})$. For jet geometry $a_{\rm jet} \leqslant 1/3$, one finds that $\nu_{\rm trans} \approx 10^{13}$ Hz; however, $\nu_{\rm trans}$ drops sharply for higher values of $a_{\rm jet}$: for $a_{\rm jet} = 0.40$, $\nu_{\rm trans} \approx 10^{10}$ Hz, while for $a_{\rm jet} = 0.45$, $\nu_{\rm trans} \approx 10^6$ Hz.

3.3. Observed Break Frequencies from Synchrotron Emission Along the Jet

The analysis carried out above implies that the observed flux from the entire jet (as opposed to a single jet segment) is characterized by several break frequencies. We present here a general discussion on the nature of these break frequencies. This is done in order to establish a general basis for the detailed discussion on the various models (Maxwellian versus power law, pure synchrotron versus adiabatic, etc.) discussed in the following sections.

We are able to identify five observed break frequencies. However, some of these frequencies are pronounced only under certain conditions. These frequencies are as follows.

1. $\nu_{\rm peak,0}$ (Equation (4)). This break frequency is inherent to any model that contains a low-energy Maxwellian distribution, and is therefore expected in all the scenarios considered.
2. $\nu_{\rm max,0}$ (Equation (8)) is expected in models in which a power-law distribution of the accelerated electrons exists, since any acceleration model necessarily has a high-energy cutoff.
3. When the magnetic field is higher than a minimum value, the electrons at the high end of the distribution rapidly cool. As a result, the cooled electrons at the base of the jet (with Lorentz factor γ_f given by Equation (17)) emit synchrotron radiation at characteristic frequency $\nu_f = (3/4\pi)(qB_0/m_e c)(\gamma\beta)_f^2$. In determining the observed frequency, one needs to discriminate between the different cases. For a Maxwellian distribution and $B_{\rm cr,1} < B_0 < B_{\rm cr,2}$, $\nu_{{\rm peak},f} > \nu_{{\rm thick},f}$, and therefore emission at $\nu_{{\rm peak},f}$ is not obscured. Thus, in this case

$$\nu_{\rm fast}(B_0 \leqslant B_{\rm cr,2}) \equiv \nu_{{\rm peak},f} = \frac{3\theta_{{\rm el},f}^2}{4\pi}\frac{qB_0}{m_e c} \simeq 1.6 \times 10^{14}\, (2a_{\rm jet} - 1)^2\, \bar{u}_0^{-3/2} \times r_{0,1}^3\, \epsilon_{B,-3}^{-3/2}\, (\gamma_j/2)^2\, (x_0/45r_s)^{-2}{\rm Hz}. \quad (26)$$

Note that while Equation (26) was derived for a Maxwellian distribution, it holds for a power-law distribution as well as long as $B_{\rm cr,0} < B_0 < B_{\rm cr,2}$, when $\theta_{{\rm el},f}$ is replaced by $(\gamma\beta)_f$. For a stronger magnetic field, $B_0 > B_{\rm cr,2}$, the electrons rapidly cool to temperature below the critical temperature $\theta_{\rm cr}$ (see Equation (18)). Once this happens, the peak of the synchrotron emission is in the optically thick regime, and is therefore obscured: $\nu_{{\rm peak},f} < \nu_{{\rm thick},f}$. The observed break in the flux therefore occurs at the transition frequency from the optically thin to the optically thick emission. By definition, this transition frequency occurs as the electrons cool to $\theta_{\rm cr}$. Emission from electrons at this temperature peaks at frequency

$$\nu_{\rm fast}(B_0 \geqslant B_{\rm cr,2}) = \frac{3\theta_{\rm el,cr}^2}{4\pi}\frac{qB_0}{m_e c} \simeq 4.0 \times 10^{14} \times \bar{u}_0^{7/10}\, r_{0,1}^{-1}\, \epsilon_{B,-3}^{3/10}\ {\rm Hz}. \quad (27)$$

4. When adiabatic energy losses are included, or for narrow jets $a_{\rm jet} < 1/2$, the analysis in Section 3.2 shows that for $B_0 < B_{\rm cr,2}$ there exists a transition frequency $\nu_{\rm trans}$, whose value was calculated in Equations (23)–(25). For high value of the magnetic field, $B_0 > B_{\rm cr,2}$, the emission peak is in the optically thick part of the spectrum already during the initial rapid cooling. As a result, in this case $\nu_{\rm trans} = \nu_{\rm fast}(B_0 \geqslant B_{\rm cr,2})$, as is defined in Equation (27).

5. The last transition frequency, which we denote here as $\nu_{\rm low}$, is relevant in a scenario of power-law energy injection, when adiabatic energy losses (or narrow jets) are considered. Cooling of the electrons at the highest end of the distribution implies that the peak frequency of synchrotron emission from these electrons, $\nu_{\rm max}(x)$, decays in a similar way to the decay of $\nu_{\rm peak}$: for wide jets with adiabatic energy losses, asymptotically $\nu_{\rm max}(x) \propto x^{-7a_{\rm jet}/3}$. This decay is faster than the decay of $\nu_{\rm thick}$, and therefore at a given distance along the jet $x_{\rm low}$, these two frequencies become similar, and equal to $\nu_{\rm low}$. Since $\gamma_{\rm max} > \gamma_{\rm min}$, necessarily $x_{\rm low} \geqslant x_{\rm trans}$, and hence $\nu_{\rm low} \leqslant \nu_{\rm trans}$. We further note that if $B_0 > B_{\rm cr,1}$, then at the end of the rapid cooling, all the electrons with initial Lorentz factor above $\gamma_{\rm min}$ cool to the same Lorentz factor, γ_f. As a result, in this case $\nu_{\rm low} = \nu_{\rm trans}$.

We therefore concentrate on the regime $B_0 < B_{\rm cr,1}$. Equation (21) gives the decay law of $\nu_{\rm thick}$ under the assumption of Maxwellian energy distribution, and is therefore valid as long as $\nu_{\rm thick} < \nu_{\rm peak}$, or equivalently $x < x_{\rm trans}$. At larger distances $x > x_{\rm trans}$, the decay law of $\nu_{\rm thick}$ is modified and depends on the power-law index p of the accelerated electrons.

In calculating the decay law of $\nu_{\rm thick}$ in this case, we largely follow the treatment by Kaiser (2006). The electron number density between $\gamma_{\rm min}$ and $\gamma_{\rm max}$ can be written as $n_{\rm el}(\gamma)d\gamma = k(x)\gamma^{-p}d\gamma$. Conservation of particles' numbers along the jet can be written as $k(x)\gamma^{-p}d\gamma = (\Delta V_0/\Delta V)k(x_0)\gamma_0^{-p}d\gamma_0$, where ΔV is the volume occupied by the electrons and the subscript "0" refers to the values at $x = x_0$. Using Equation (2) for adiabatic energy losses along the jet and using $\Delta V \propto r^2$, one finds that $k(x) = k(x_0)(r/r_0)^{-(2p+4)/3}$.

In this case of a power-law distribution, the emissivity is $j_\nu \propto kB^{(p+1)/2}\nu^{-(p-1)/2}$ and the optical depth is $\tau_\nu \propto rkB^{(p+2)/2}\nu^{-(p+4)/2}$ (e.g., Rybicki & Lightman 1979). Using $\nu_{\rm thick} = \nu|_{\tau_\nu=1}$, one finds

$$\nu_{\rm thick} \propto \left(krB^{(p+2)/2}\right)^{2/(p+4)} \propto r^{-\hat{A}_1}, \quad (28)$$

where $\hat{A}_1(p) = (8+7p)/3(p+4)$. We emphasize that this decay law of $\nu_{\rm thick}$ is relevant only for $x > x_{\rm trans}$, while at smaller radii, the analysis carried out in Section 3.2 holds.

Repeating a similar analysis to the one carried out in Section 3.2, one finds that for $B_0 < B_{\rm cr,0}$,

$$\nu_{\rm low} \approx 2.6\times10^5\ \bar{u}_0^{(3\hat{A}_2/16)(5-\hat{A}_1)}\ r_{0,1}^{-15\hat{A}_2/16}\ \epsilon_{e,0}^{(\hat{A}_2/8)(15\hat{A}_1-19)} \times \epsilon_{B,-3}^{(\hat{A}_2/16)(2\hat{A}_1+1)}{\rm Hz}, \approx 2.6\times10^5\ \bar{u}_0^{2.5}\ r_{0,1}^{-2}\ \epsilon_{e,0}^{-10}\ \epsilon_{B,-3}^{-0.4}\ {\rm Hz}, \quad (29)$$

where $\hat{A}_2(p) = (7/3)/[(7/3)+\hat{A}_1(p)]$, and the second line gives the approximate dependence for p in the range $2.0 \leqslant p \leqslant 2.5$.

Similarly, for $B_{\rm cr,0} < B_0 < B_{\rm cr,1}$,

$$\nu_{\rm low} \approx 10^{12}\ \bar{u}_0^{4.25}\ r_{0,1}^{-5.5}\ (\gamma_j/2)^{-2}\ (x_0/45r_s)^2\ \epsilon_{B,-5}^{1.5}\ {\rm Hz}. \quad (30)$$

Calculation of $\nu_{\rm low}$ for narrow jets, $a_{\rm jet} < 1/2$, is straightforward, yet cumbersome. For $2.0 \leqslant p \leqslant 2.5$ and $a_{\rm jet} \lesssim 0.1$, we find $\nu_{\rm low} \approx 10^{12}$ Hz, while for wider jets, $\nu_{\rm low}$ rapidly decays: $\nu_{\rm low} \approx 10^{10}$ Hz for $a_{\rm jet} = 0.2$, and $\nu_{\rm low} \approx 10^7$ Hz for $a_{\rm jet} = 1/3$. As we will show in Section 8, for narrow jets it is impossible to obtain a flat spectrum at the radio band, as suggested by observations. Therefore, we will give only a brief explanation on the possible spectrum obtained in this scenario.

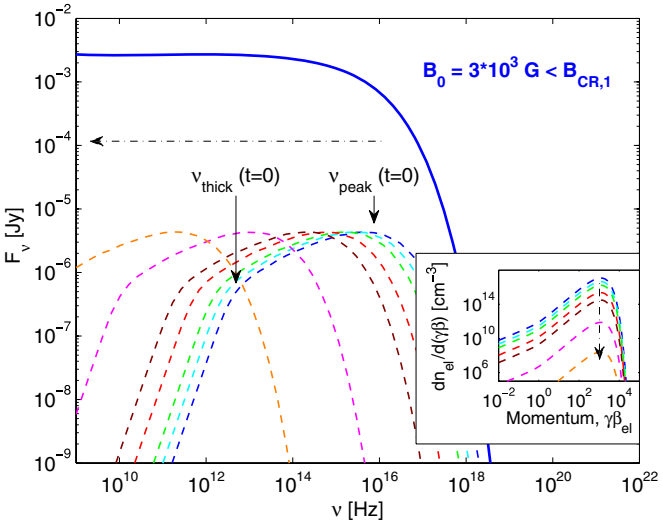

Figure 2. Example of the spectra obtained from an initial Maxwellian distribution of electrons radiating in a weak magnetic field, $B_0 = 3\times10^3\ {\rm G} < B_{\rm cr,1}$, when adiabatic energy losses are neglected. The values of the free model parameters are the same as the "canonical" values taken in Section 2.1.1. Thus, we consider flow parameters resulting in $\bar{u}_0 = 1$, $x_0 = 45r_s$, $r_0 = 10r_s$, and $\epsilon_{e,0} = 1$. We further consider a conical jet, $a_{\rm jet} = 1$. As the distance to the object we take the distance to XTE J1118+480, $d = 1.8$ kpc. The inner panel shows the electrons' energy distribution at increasing distances along the jet. As the electrons' temperature is nearly constant, their density decays as $n_{\rm el,tot} \propto r^{-2}$. In the main panel we show the resulting flux (solid line), and its decomposition into the flux emitted from the different jet segments (dash lines). Marked in arrows are the characteristic frequencies $\nu_{\rm peak,0}$ and $\nu_{\rm thick,0}$. These frequencies are clearly seen when looking at emission from arbitrary jet segments at $x > x_0$, however, the overall spectra below $\nu_{\rm peak,0}$ are flat, $F_\nu \propto \nu^0$ (for $a_{\rm jet} = 1$, see the text). The dash-dotted arrows show the direction of the evolution of the electron distribution and the emitted flux at different times, which are equivalent to distance along the jet.

(A color version of this figure is available in the online journal.)

We further discuss the role of these five transition frequencies on the observed spectrum in the following sections, when we present a detailed analysis of the various spectra that can be obtained. The transition frequencies are marked in Figures 2–9 when discussing the various possibilities.

4. EMISSION FROM INITIAL MAXWELLIAN DISTRIBUTION OF ELECTRONS WITHOUT ADIABATIC COOLING

In this section, we present the results of a model that includes only synchrotron cooling of the electrons, i.e., we neglect adiabatic energy losses. While adiabatic energy losses occur as the gas expands, both the formation and confinement mechanisms of jets are still not fully understood. It could thus be that the expansion of particles inside the jet is not purely adiabatic, and that the electrons are heated as they propagate along the jet (e.g., by lateral shock waves). Neglection of the adiabatic energy losses can thus be considered as an extreme, yet still physically plausible, scenario.

We further concentrate in this section on a scenario in which the acceleration process results in a Maxwellian distribution of the energetic electrons. This assumption both has theoretical motivation and is used for illustrative purposes. From a theoretical perspective, as discussed in Section 1, the mechanism that accelerates particles to high energies (e.g., via shock waves) is not understood from first principles. While it is likely that some fraction of the electrons are accelerated to a high-energy power-law tail above the peak of the Maxwellian, the fraction

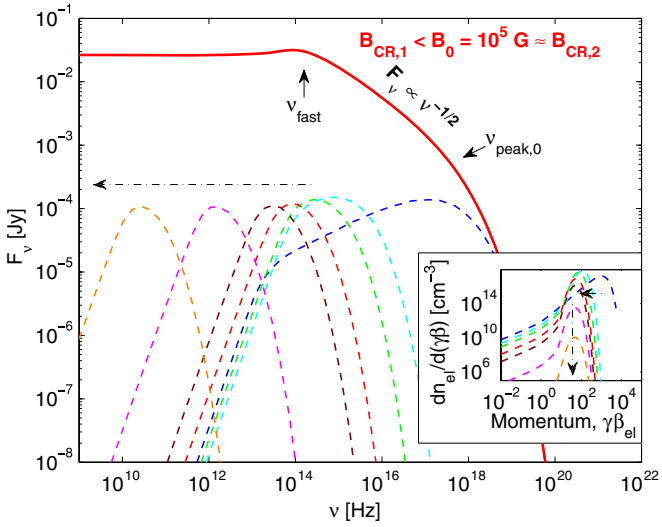

Figure 3. Example of the spectra obtained from an initial Maxwellian distribution of electrons radiating in an intermediate magnetic field, $B_{\rm cr,1} < B_0 = 10^5$ G $\approx B_{\rm cr,2}$, when adiabatic energy losses are neglected. Apart from the magnetic field, all the other parameter values are the same as in Figure 2. Inner panel: electron energy distribution at different regions in the jet. The dash-dotted arrows show the temporal evolution: at first the electrons rapidly cool close to the jet base, while maintaining an approximate Maxwellian distribution. At a later stage, the electron number density decreases as $n_{\rm el,tot} \propto r^{-2}$. Main panel: the resulting spectrum (solid line) and a decomposition to the spectrum emitted from different segments (dashed lines). We mark the transition frequencies $\nu_{\rm peak,0}$ and $\nu_{\rm fast}$. The initial rapid electron cooling results in a fast decay of $\nu_{\rm peak}(t)$, which leads to a flux decay $F_\nu \propto \nu^{-1/2}$ at the range $\nu_{\rm fast} < \nu < \nu_{\rm peak,0}$. Following the rapid decay, the two characteristic frequencies $\nu_{\rm thick}$ and $\nu_{\rm peak}$ have nearly the same values (see the text) and evolve in a similar way along the jet, as is seen by the decomposition. As a result, below $\nu_{\rm fast}$, the flux decays in a similar way to the decay in the weak magnetic field scenario, described in Figure 2.

(A color version of this figure is available in the online journal.)

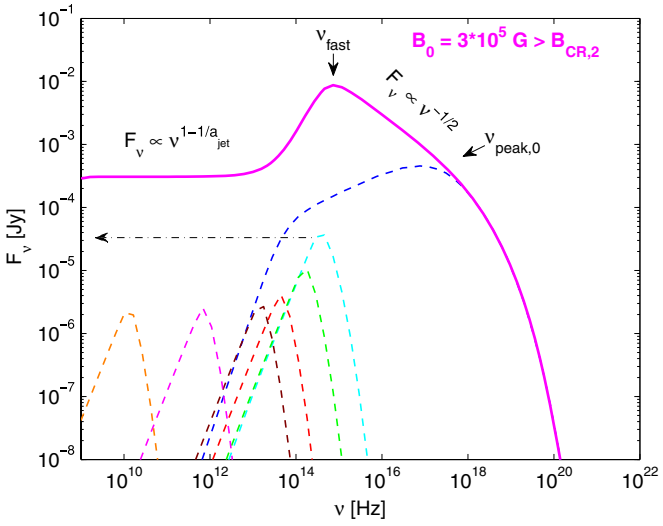

Figure 4. Example of the spectra obtained from an initial Maxwellian distribution of electrons radiating in a strong magnetic field, $B_0 = 3 \times 10^5$ G $> B_{\rm cr,2}$, when adiabatic energy losses are neglected. All the other parameters are the same as in Figure 2. Clearly, the flux at high frequencies, $\nu > \nu_{\rm fast}$, is similar to the case of a lower magnetic field (see Figure 3), while at low frequencies, below $\nu_{\rm fast}$, the flux is strongly suppressed. The decomposition of the flux to emission from the different jet segments reveals that the origin of this suppression is the suppression of emission from the different segments, which are in the optically thick regime following the initial rapid cooling. The dash-dotted arrow shows the temporal evolution of the emitted flux along the jet. Clearly, emission at high frequencies is from electrons during their initial fast cooling phase, and therefore the only effect of the strong magnetic field is a shift in $\nu_{\rm fast}$ (see the text for details). The electrons' temporal evolution is very similar to the one presented by the inner panel in Figure 3, and is thus omitted.

(A color version of this figure is available in the online journal.)

of electrons in the energetic tail is uncertain. Thus, we consider this scenario as being a physically plausible scenario of electron acceleration process. In addition, studying this scenario is helpful for understanding the spectral dependence on the uncertain value of the magnetic field and possible jet geometries. We expand our model in Section 5 to the cases of power-law distribution of the energetic electrons and to consider adiabatic energy losses.

Here and in Sections 5–7, we focus on scenarios of wide jets. A narrow jet scenario is discussed in Section 8.

4.1. Weak Magnetic Field: Production of Flat Radio Spectra in Conical Jets

For a weak magnetic field at the jet base, $B_0 < B_{\rm cr,1}$, and for wide jets, $a_{\rm jet} > 1/2$, electron cooling is insignificant in the entire jet (this scenario is illustrated in Figure 1; $B_0 = 10^4$ G). The insignificance of electron cooling implies that the electrons' temperature $\theta_{\rm el}$ is constant along the jet, $\theta_{\rm el}(x) \simeq \theta_{\rm el,0}$. The peak and break frequencies thus decay in accordance with Equation (20), $\nu_{\rm peak} \propto \nu_{\rm thick} \propto x^{-a_{\rm jet}}$.

The observed flux at frequency $\nu \leqslant \nu_{\rm peak,0}$ can be calculated by integrating the emitted flux from the different jet segments (this is illustrated in Figure 2). In order to carry out an analytical calculation, we approximate emission from a jet segment at position $x...x + dx$ as contributing only at frequencies $\nu \leqslant \nu_{\rm peak}(x)$ (at higher frequencies the flux decays exponentially). The decay of the magnetic field implies that the peak frequency $\nu_{\rm peak}(x)$ decays along the jet. Therefore, at a given frequency $\nu \leqslant \nu_{\rm peak,0}$, the contribution to the flux is from jet regions only up to a position $x_{\rm max}$ for which $\nu_{\rm peak}(x_{\rm max}) = \nu$. The decay law of the magnetic field thus gives $x_{\rm max} = x_0[\nu/\nu_{\rm peak,0}]^{-1/a_{\rm jet}}$. Using the contribution to the flux from the optically thin regions of the spectrum (Equation (11)) one obtains

$$F_\nu \simeq \frac{2r_0^2 A_0}{9d^2}\frac{\theta_{\rm el_0}^3 q^3 B_0}{m_e c^2}\int_{x_{\rm min}}^{x_{\rm max}}\left(\frac{x}{x_0}\right)^{-a_{\rm jet}}\left(\frac{3\nu}{4\nu_{\rm peak,0}}\right)^{1/3}\left(\frac{x}{x_0}\right)^{a_{\rm jet}/3} dx$$
$$= \left(\frac{3}{4}\right)^{1/3}\frac{2r_0^2}{9d^2}\frac{u_0 q^3 B_0 x_0}{(1-2a_{\rm jet}/3)m_e c^2 m_p c^2}\left(\frac{\nu}{\nu_{\rm peak,0}}\right)^{1-1/a_{\rm jet}}. \quad (31)$$

The lower integration boundary is taken here as $x_{\rm min} = x_0$; however, the exact boundary is irrelevant as long as $x_{\rm max} \gg x_{\rm min}$. We thus conclude that for a weak magnetic field, the observed flux at $\nu < \nu_{\rm peak,0}$ depends on the jet geometry via $F_\nu \propto \nu^{1-1/a_{\rm jet}}$ (see Figure 2).

For a conical jet, $a_{\rm jet} = 1$, we therefore find that the flux below $\nu_{\rm peak,0}$ is constant (i.e., a flat spectrum, $F_\nu \propto \nu^0$). While this result is similar to the result first obtained by Blandford & Königl (1979), here it has a different physical origin. In Blandford & Königl (1979), the origin of the flat radio spectrum is the decay of the break frequency $\nu_{\rm thick}$ along the jet, while here it is the decay of peak frequency, $\nu_{\rm peak}$. The decay law of the break frequency is similar to that of the peak frequency, and thus its existence cannot be observed when the integrated flux along the jet is considered.

We further point out that in this regime of $B_0 < B_{\rm cr,1}$, the total (integrated) observed flux below $\nu_{\rm peak,0}$ linearly depends on B_0, and on the position of the jet base, x_0. We show in Figure 2 the results of an exact numerical calculation of the observed flux and its decomposition to emission from different jet segments

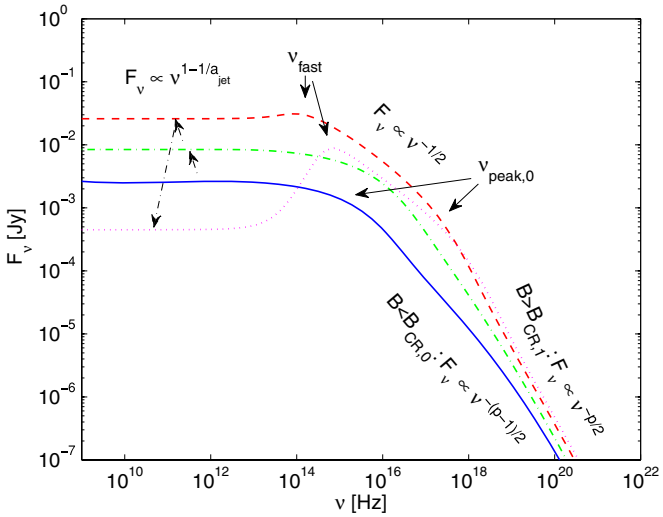

Figure 5. Examples of spectra obtained from an initial power-law distribution of electrons with power-law index $p = 2.5$, for various values of the magnetic field, around the critical values $B_{cr,1}$ and $B_{cr,2}$: $B_0 = 3 \times 10^3$ G (solid, blue), 10^4 G (dash-dotted, green), 10^5 G (dash-dash, red), and 3×10^5 G (dotted, purple). Adiabatic energy losses are neglected here. All the other parameters are the same as in Figure 2. The key result here is that an increase in the magnetic field above $B_{cr,2}$ decreases the radio spectra, with only a minor effect on the spectra at the X-ray band. Marked are the transition frequencies $\nu_{peak,0}$ and ν_{fast}. For $B_0 > B_{cr,2}$, ν_{fast} increases with B_0 (see Equation (27)). The dashed arrows indicate the evolution of the spectra with the increase in the magnetic field. At low frequencies, below $\nu_{peak,0}$, the spectra obtained from Maxwellian distribution (Section 4) for similar values of the magnetic field are similar to that obtained here. At higher frequencies, above $\nu_{peak,0}$, the spectral slope gradually changes from $(p-1)/2$ for $B_0 < B_{cr,0}$ to $p/2$ for $B_0 > B_{cr,1}$.

(A color version of this figure is available in the online journal.)

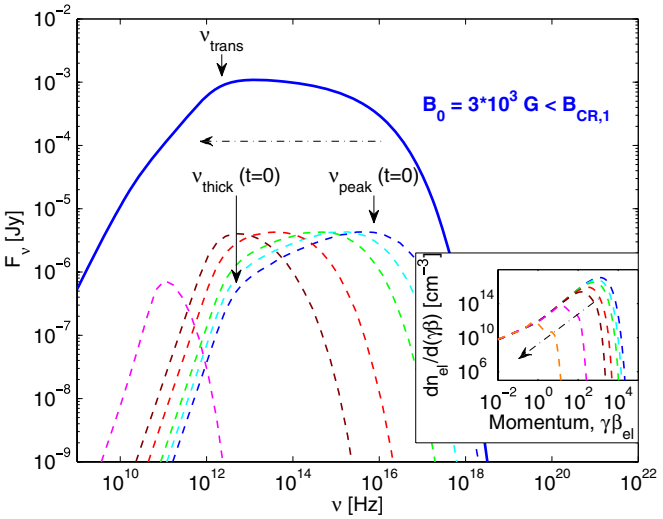

Figure 6. Example of the spectra obtained from an initial Maxwellian distribution of electrons radiating in weak magnetic field, $B_0 = 3 \times 10^3$ G $< B_{cr,1}$, when adiabatic energy losses are considered. All the other parameters are the same as in Figure 2. The dash-dotted arrows show the direction of the evolution of the electron distribution (inner inset) and flux (main panel). The electrons main cooling mechanism is adiabatic energy losses, which result in $\theta_{el} \propto x^{-2a_{jet}/3}$. The transition frequency ν_{trans} is clearly marked. The decomposition into emission from jet segments illustrates that the transition occurs once the emission from the jet segments becomes optically thick, above x_{trans} (see Equation (22)). At $\nu_{trans} < \nu < \nu_{peak,0}$, $F_\nu \propto \nu^{(3/7)(1-1/a_{jet})}$, which for $a_{jet} = 1$ as considered here results in flat spectra. However, below ν_{trans} a flat spectra cannot be obtained (see the text for details).

(A color version of this figure is available in the online journal.)

obtained in this case. The details of the numerical code are given in the Appendix.

4.2. Intermediate Magnetic Field: Spectral Slope $F_\nu \propto \nu^{-1/2}$ at the Optic/UV Bands

In this section, we consider an intermediate magnetic field at the jet base, $B_{cr,1} < B_0 < B_{cr,2}$. By definition, for $B_0 > B_{cr,1}$ the electrons rapidly cool close to the jet base (see Section 3.1, Equations (15)), while the requirement $B_0 < B_{cr,2}$ implies that at the end of the rapid cooling phase, still $\nu_{thick} < \nu_{peak}$ (see Equation (19)). The rapid cooling introduces an additional break frequency in the observed spectrum, ν_{fast} (see Section 3.3, Equation (26), and Figure 3).

As explained in Sections 2.3 and 3.3, in this case of initial rapid cooling, the analytical calculations are carried out in two steps. We first calculate the emissivity during the rapid cooling phase, under the assumption that the magnetic field is constant during this phase, and is equal to B_0. Emission at this phase contributes to the flux at the frequency range $\nu_{fast} \leqslant \nu \leqslant \nu_{peak,0}$. At a second step, we calculate the emissivity during the rest of the electron propagation along the jet, assuming that their temperature is constant in this phase (given by Equation (17)), and that only the magnetic field decays. At this stage, the electron emission contributes to the flux at lower frequencies $\nu < \nu_{fast}$. The results of the full numerical calculations presented in Figure 3 confirm the validity of the analytical approximations.

The flux at $\nu_{peak,0}$ is estimated by assuming that the entire electron distribution is concentrated at a single energy (characterized by Lorentz factor γ_{min}) and that the emission in monochromatic, at $\nu_{peak,0}$. Thus, the total power emitted at $\nu_{peak,0}$ is $P_\nu|_{\nu=\nu_{peak,0}} \simeq P_0/\nu_{peak,0} = 16\pi q^3 B_0/27 m_e c^2 \Lambda$. Here, $P_0 = 4q^4 B_0^2 (\gamma\beta)_{min}^2/9m_e^3c^5$ is the total power emitted, and the factor $\Lambda \approx 10$ is introduced here to account for the distribution in the electron energy and for the fact that the emission is not monochromatic. The emissivity is $j_\nu|_{\nu=\nu_{peak,0}} = n_{el,tot} \times P_\nu|_{\nu=\nu_{peak,0}}/4\pi$ where $n_{el,tot} \approx u_0/m_p c^2$ is the number density of electrons at the base of the jet. The observed flux from a segment of length Δx close to the base of the jet is therefore

$$\Delta F_\nu|_{\nu=\nu_{peak,0}} = \frac{r_0^2}{2d^2}\frac{4q^3 B_0}{27 m_e c^2 \Lambda}\frac{u_0}{m_p c^2}\Delta x. \quad (32)$$

Comparison with Equation (31) derived in Section 4.1 indeed shows that the results are similar up to a numerical factor. However, the estimate here is based on robust arguments, that can be (and will be) generalized in studying the flux in the power-law scenario discussed below.

The length Δx at which electron radiation contributes to the flux at $\nu_{peak,0}$ can be estimated by the characteristic time it takes the electrons to lose their energy (Equation (14)). Since the energy loss is very rapid and occurs within time $t \gtrsim t_0$, one can approximate the energy loss time in the following way. Defining $\epsilon = t/t_0 - 1 = x/x_0 - 1$, one finds that for $\epsilon \ll 1$, Equation (14) can be written in the form

$$\gamma\beta(t \gtrsim t_0) \simeq \frac{\gamma\beta(t_0)}{1 + \frac{4\sigma_T}{3m_e c}\frac{B_0^2}{8\pi}\gamma\beta(t_0)t_0\epsilon} \approx \frac{6\pi m_e c}{\sigma_T B_0^2 t_0 \epsilon}, \quad (33)$$

where the last equality holds for $\epsilon \gg 6\pi m_e c/\sigma_T B_0^2 \gamma\beta(t_0)t_0$.[4] The characteristic energy loss time of electrons with initial

[4] Note that for $B_0 > B_{cr,1}$, by definition, $6\pi m_e c/\sigma_T B_0^2 \gamma\beta(t_0)t_0 < 1$, and thus the solution is valid.

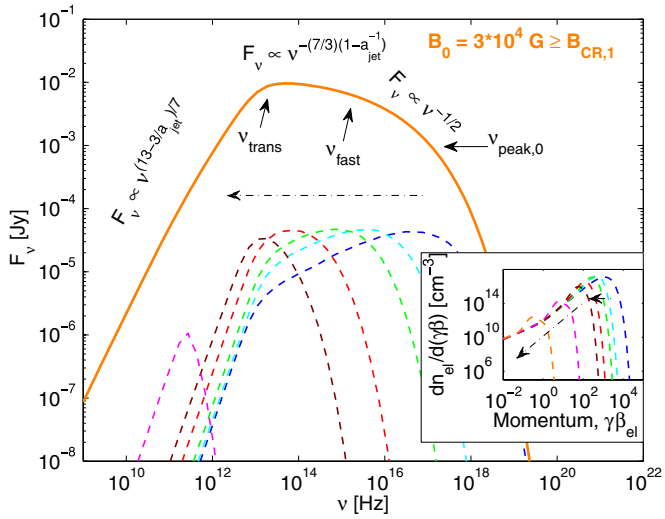

Figure 7. Example of the spectra obtained from an initial Maxwellian distribution of electrons radiating in an intermediate magnetic field, $B_{cr,1} \lesssim B_0 = 3 \times 10^4\,\mathrm{G} < B_{cr,2}$, when adiabatic energy losses are considered. All the other parameters are the same as in Figure 2. The dash-dotted arrows show the direction of the evolution of the electron distribution (inner inset) and flux (main panel). The initial rapid decay of the electrons temperature is seen in the inner panel. While we mark in this figure the three transition frequencies, $\nu_{peak,0}$, ν_{fast}, and ν_{trans}, clearly for an intermediate value of B_0 the transition in the flux behavior is smooth.

(A color version of this figure is available in the online journal.)

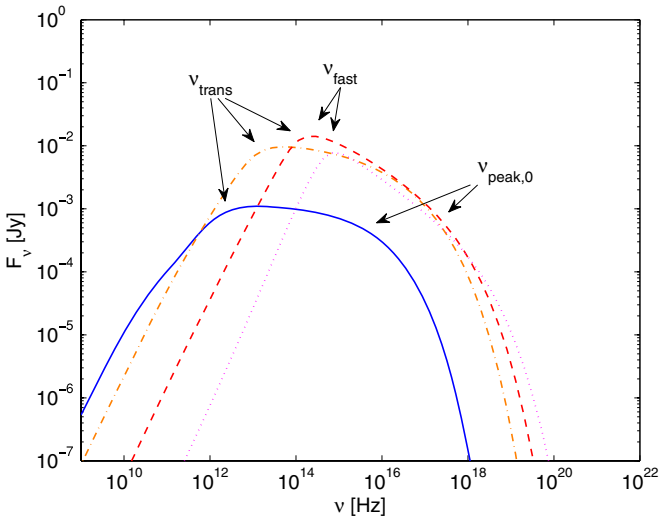

Figure 8. Example of spectra obtained from an initial Maxwellian distribution of electrons when adiabatic energy losses are included, for various values of the magnetic field, around the critical values $B_{cr,1}$ and $B_{cr,2}$: $B_0 = 3 \times 10^3$ G (solid, blue), 3×10^4 G (dash-dotted, orange), 10^5 G (dash-dash, red), and 3×10^5 G (dotted, purple). All the other parameters are the same as in Figure 2. As the magnetic field increases, ν_{trans} shifts to higher frequencies, and for $B_0 \geqslant B_{cr,2}$, $\nu_{trans} = \nu_{fast}$. As a result, flat radio spectra cannot be obtained at low frequencies in this model. The increase in the magnetic field results in a shift of ν_{fast} to higher frequencies, as predicted by Equation (27). For $B_0 > B_{cr,1}$, the flux at higher frequencies is nearly insensitive to the exact value of the magnetic field.

(A color version of this figure is available in the online journal.)

momentum $\gamma\beta(t_0)$ can therefore be written as

$$\Delta t = t_0 \epsilon \approx \frac{6\pi m_e c}{\sigma_T B_0^2 \gamma\beta(t_0)}. \quad (34)$$

Writing $\Delta x = \gamma_j \beta_j c \Delta t$ and using this result in Equation (32), one finds that the flux at $\nu_{peak,0}$ is

$$F_\nu|_{\nu=\nu_{peak,0}} = \frac{4q^3 q_j \dot{M}_{disk}}{27 d^2 m_p c \sigma_T B_0 \theta_{el,0} \Lambda}. \quad (35)$$

At frequencies below $\nu_{peak,0}$ and above ν_{fast}, the flux can be calculated as follows. At this frequency range, the flux is dominated by emission from electrons during their initial rapid cooling phase. As the electrons cool, the peak of the synchrotron emission $\nu = \nu_{peak}(t)$ decays. The power emitted at ν, $P_\nu|_{\nu_{peak}(t)}$ is independent of the electron energy (see discussion and Equation (32); note that since $B = B_0$ is constant, Equation (32) is in fact valid for emission at all the frequencies in the range $\nu_{fast} \leqslant \nu \leqslant \nu_{peak,0}$, when the appropriate length Δx is taken). Therefore, the observed flux at these frequencies $F_\nu(\nu_{fast} < \nu < \nu_{peak,0})$ depends only on the electron cooling time, or cooling length Δx, during which synchrotron emission contributes to the flux at frequency ν. Using the decay law of the electron energy at early times derived above (Equation (33)), one finds $\gamma\beta(t) \propto (t_0\epsilon)^{-1} \propto \Delta x^{-1}$. The peak emission frequency depends on the electron momentum via $\nu = \nu_{peak}(t) \propto B(\gamma\beta)^2(t) \propto \Delta x^{-2}$. We therefore conclude that $\nu(t) \propto \Delta x^{-2}$. Again using Equation (32), one immediately concludes that since $F_\nu \propto \Delta x$, then for $\nu_{fast} \leqslant \nu \leqslant \nu_{peak,0}$ the flux decays as $F_\nu \propto \nu^{-1/2}$. Note that this result is independent of the jet geometry.

Once the electrons cool to their asymptotic temperature, $\theta_{el,f}$, they continue to propagate along the jet without further significant energy losses. For intermediate value of the magnetic field, $B_{cr,1} \leqslant B_0 \leqslant B_{cr,2}$, in spite of their cooling, still $\nu_{thick} < \nu_{peak}$. As a result, at low frequencies $\nu < \nu_{fast}$, the analysis of the flux carried out in Section 4.1 holds. In particular, we conclude that for $\nu < \nu_{fast}$, $F_\nu \propto \nu^{1-1/a_{jet}}$, and that the flux at these frequencies linearly depends on B_0 and x_0.[5]

Examples of the spectrum are presented in Figure 3. In the inner inset, we show the electron energy distribution in different regions along the jet (the arrows indicate the direction of the temporal or equivalently the spatial evolution). In spite of the early, rapid cooling, still the electrons maintain a quasi-Maxwellian distribution along the jet, with asymptotic temperature given by Equation (17). The main panel shows the observed flux, and its decomposition into the flux emitted from the different segments along the jet. The flux decay $F_\nu \propto \nu^{-1/2}$ at the range $\nu_{fast} < \nu < \nu_{peak,0}$ is pronounced. As can be seen by the decomposition, contribution to the flux at these frequencies is only from the innermost parts of the jet.

4.3. Strong Magnetic Field: Suppression of the Flux at Radio Frequencies

If the magnetic field at the jet base is higher than $B_{cr,2}$, then the electrons rapidly cool to a temperature below the critical temperature θ_{cr} (see Equation (18)). Once this happens, the peak of the synchrotron emission is in the optically thick region, and is therefore obscured, $\nu_{peak} < \nu_{thick}$. The observed break frequency ν_{fast} in this case is given by emission from electrons at θ_{cr} and has been calculated in Section 3.3, Equation (27).

Emission at lower frequencies that occurs as the electrons continuously cool below θ_{cr} is obscured, since it is in regions of

[5] The linear dependence of the flux below ν_{fast} on B_0 can be derived indirectly, from the analysis carried out above. It is an immediate consequence of the facts that $\nu_{peak,0} \propto B_0$, $F_\nu|_{\nu_{peak,0}} \propto B_0^{-1}$, $\nu_{fast} \propto B_0^{-3}$, and $F_\nu|_{\nu_{fast}<\nu<\nu_{peak,0}} \propto \nu^{-1/2}$.

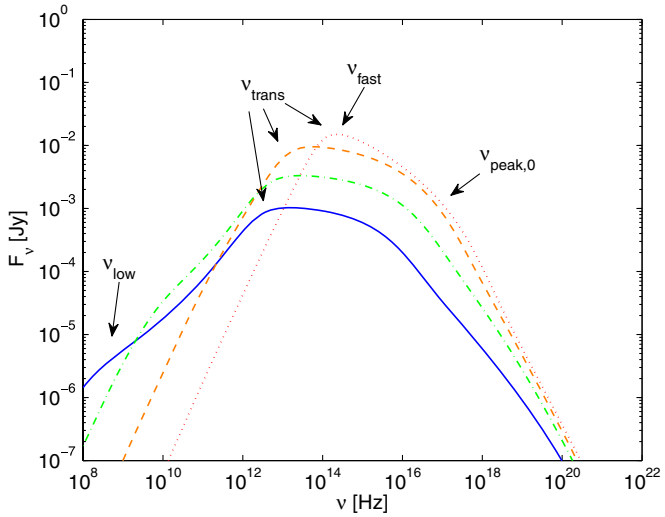

Figure 9. Examples of spectra obtained from an initial power-law distribution of electrons with power-law index $p = 2.5$ when adiabatic energy losses are included, for various values of the magnetic field, around the critical values $B_{cr,1}$ and $B_{cr,2}$: $B_0 = 3 \times 10^3$ G (solid, blue), 10^4 G (dash-dotted, green), 3×10^4 G (dash-dash, orange), and 10^5 G (dotted, red). All the other parameters are the same as in Figure 2. We mark the transition frequencies $\nu_{peak,0}$, ν_{fast}, ν_{trans}, and ν_{low}. At the frequency range $\nu_{low} < \nu < \nu_{trans}$, the flux dependence on the jet geometry is described in Equation (41). At other frequencies the spectral shape is similar to the spectral shape discussed in former sections. In particular, the steepening of the slope at high frequencies from $(p-1)/2$ to $p/2$ with the increase in B_0 is pronounced.

(A color version of this figure is available in the online journal.)

high optical depth ($\nu_{peak} < \nu_{thick}$). As a result, for $B_0 > B_{cr,2}$ the peak of the observed flux is at frequency ν_{fast} given by Equation (27), while at lower frequencies the flux decays. We therefore conclude that further increase in the magnetic field above $B_{cr,2}$ results in an increase in the observed spectral break frequency, ν_{fast}, in accordance with the dependence given in Equation (27) (as opposed to the result obtained for $B_{cr,1} \leqslant B_0 \leqslant B_{cr,2}$; see Equation (26)).

Similar to the scenario presented in Section 4.2, in a strong magnetic field the electrons lose most of their energy rapidly. Thus, the calculation of the flux at $\nu_{peak,0}$ in Equation (35) holds. Similarly, below $\nu_{peak,0}$ and above ν_{fast}, the flux decays as $F_\nu \propto \nu^{-1/2}$.

At lower frequencies, radio-IR, emission is dominated by electrons propagating along the jet with temperature $\theta_{el,f} < \theta_{cr}$. Emission from these electrons is characterized by $\nu_{peak}(x) < \nu_{thick}(x)$. For a Maxwellian distribution of electrons, above ν_{peak} the flux decays exponentially. Thus, an exact calculation of ν_{thick} requires solving a transcendental equation. Using the results of Jones & Hardee (1979) for $z \gg 1$ (see discussion below Equation (4)), and the optical depth given in Equation (5), the break frequency ν_{thick} can be calculated by solving the Equation $[3\nu_{thick}(x)/2\nu_{peak}(x)]^{1/3} = (2/3)\log[\pi^2 r(x) A q^2 c/4\nu_{thick}(x)]$. Here, we approximate the logarithm on the right-hand side as constant, which enables us to write $\nu_{thick}(x) = \alpha\nu_{peak}(x)$. The parameter α depends on B_0. We find numerically that α has a characteristic value of a few tens ($\alpha \approx 3$ for $\epsilon_B \simeq \epsilon_{B,cr,2}$, $\alpha \approx 60$ for $\epsilon_B = 10\epsilon_{B,cr,2}$, and $\alpha \approx 100$ for $\epsilon_B = 100\epsilon_{B,cr,2}$).

With this approximation, one can calculate the expected flux at the radio frequencies by integrating the flux in the optically thick part of the spectrum (Equation (10)) over the different jet segments, in a similar way to the calculation of the radio flux carried out in Section 4.1. Since the electrons cool to their terminal temperature $\theta_{el,f}$ close to the jet base, at a given frequency $\nu \leqslant \nu_{thick}(x)$ emission is obtained from jet regions $x_0 \leqslant x \leqslant x_{max}$, where $x_{max} = x_0(\nu/\alpha\nu_{peak,f})^{-1/a_{jet}}$. Integrating the flux in the optically thick part of the spectrum, using Equation (10) one obtains

$$F_\nu \simeq \frac{r_0}{d^2} m_e \theta_{el,f} \nu^2 \int_{x_{min}}^{x_{max}} \left(\frac{x}{x_0}\right)^{a_{jet}} dx = \frac{r_0}{d^2} m_e \theta_{el,f} \nu_{peak,f}^2 x_0 \alpha^{1+1/a_{jet}} \left(\frac{\nu}{\nu_{peak,f}}\right)^{1-1/a_{jet}}. \quad (36)$$

We therefore find that for $B_0 > B_{cr,2}$, the radio flux *decreases* with the increase in B_0, as $F_\nu \propto \theta_{el,f}^5 B_0^2 \propto B_0^{-8} (\propto \epsilon_B^{-4})$. We find numerically that the decay law is somewhat weaker, due to the nonlinear dependence of α on B_0. We further find that the radio flux depends on the jet size as $F_\nu \propto x_0^{-4}$, and on the jet geometry in a similar way as in the weak magnetic field scenario, $F_\nu \propto \nu^{1-1/a_{jet}}$.

Example of the spectra obtained is presented in Figure 4. Clearly, the flux at high frequencies, above ν_{fast}, is similar to the flux obtained for weaker magnetic field (see Figure 3). However, at lower frequencies, mainly at the radio band, the flux is strongly suppressed due to the self-absorption. This result can naturally explain differences in radio emission that are not accompanied by similar differences at higher bands in various sources, by an adjustment of a single parameter—the magnetic field.

In Figure 5, we compare the resulting spectra for different values of the magnetic field. While this figure is derived for power-law distribution of the energetic electrons (see Section 5), the resulting flux below $\nu_{peak,0}$ is independent of the distribution of the electrons above γ_{min} and are thus similar for both cases. This figure illustrates how an increase in the magnetic field from low values first leads to an increase in the radio flux, which changes to a decrease in the observed flux when $B_0 > B_{cr,2}$. The flux at the *X* band, on the other hand, is much less sensitive to the value of the magnetic field. We further discuss the implications of this in Section 9.

5. EMISSION FROM POWER-LAW DISTRIBUTION OF ELECTRONS WITHOUT ADIABATIC COOLING

We next consider an initial distribution of the accelerated electrons in the form of a power-law energy distribution above the peak of the Maxwellian and below a maximum Lorentz factor γ_{max}, with power-law index p. Equation (14) that describes the decay of the electron momentum due to synchrotron emission is independent of the electron distribution, and hence is valid in this scenario as well. As a result, most of the analysis carried out in Section 4 is valid here. However, the inclusion of a power law implies that there is an additional critical value for the magnetic field, $B_{cr,0}$ (see Section 3.1, Equation (16)). Thus, in calculating the resulting spectrum, one needs to discriminate here also between the cases $B_0 > (<) B_{cr,0}$, since these two cases are qualitatively different. For a weak magnetic field, $B_0 < B_{cr,0}$, the electron distribution is unaffected by synchrotron cooling. In contrast, for $B_0 > B_{cr,0}$, the high-energy tail of the electron distribution is cooled significantly, while the low-energy tail may be less affected. As a result, the initial electron energy distribution is modified.

5.1. Weak Magnetic Field

We first consider a very weak magnetic field at the jet base, $B_0 < B_{cr,0}$. In this case, electron cooling in the entire energy

range is insignificant. Thus, standard synchrotron theory (e.g., Rybicki & Lightman 1979) implies that above $\nu_{\rm peak}$ and below $\nu_{\rm max}$, the power emitted by a jet segment is $P_\nu \propto \nu^{-(p-1)/2}$. The observed flux is calculated in a very similar way to the calculation of the flux done in Section 4, by integrating the contribution to the flux from the different segments along the jet. In particular, at low frequencies $\nu < \nu_{\rm peak,0}$, a similar analysis to the one carried out in Section 4.1 holds, and thus $F_\nu \propto B_0(\nu/\nu_{\rm peak,0})^{1-1/a_{\rm jet}}$. This is illustrated in Figure 5.

The arguments that led to Equation (32) can be generalized to emission at high frequencies, $\nu > \nu_{\rm peak}$, from an arbitrary jet segment at position $x...x + dx$, as long as electrons in this jet segment contribute to the emission at this frequency. One therefore finds that the contribution to the flux at high frequencies from a jet segment is given by

$$dF_\nu|_{\nu\geqslant\nu_{\rm peak}} = \frac{2q^3B}{27\pi d^2 m_e c^2\Lambda}\frac{q_j\dot{M}_{\rm disk}}{\gamma_j\beta_j m_p c}\left(\frac{\nu}{\nu_{\rm peak}}\right)^{-(p-1)/2}dx. \quad (37)$$

In order to calculate the total flux, one needs to integrate over the jet segments that contribute to the flux at a given frequency ν. Since in this case of weak magnetic field the electron energy is constant along the jet, the peak frequency decay is attributed only to the decay of the magnetic field, and $\nu_{\rm peak} = \nu_{\rm peak,0}(x/x_0)^{-a_{\rm jet}}$. The observed flux at frequency $\nu \geqslant \nu_{\rm peak,0}$ is therefore calculated by integrating the emission from jet regions $x_0 \leqslant x \leqslant x_{\rm max}$,

$$F_\nu|_{\nu\geqslant\nu_{\rm peak,0}} = \frac{2q^3B_0}{27\pi d^2 m_e c^2\Lambda}\frac{q_j\dot{M}_{\rm disk}}{\gamma_j\beta_j m_p c}\left(\frac{\nu}{\nu_{\rm peak,0}}\right)^{-\frac{(p-1)}{2}} \times\frac{x_0}{a_{\rm jet}\frac{(p+1)}{2}-1}\left[1-\left(\frac{x_0}{x_{\rm max}}\right)^{a_{\rm jet}\frac{(p+1)}{2}-1}\right]. \quad (38)$$

For a given frequency $\nu \ll \nu_{\rm max}$, contribution to the flux is from regions up to $x_{\rm max}(\nu)/x_0 = (\nu/\nu_{\rm max})^{-1/a_{\rm jet}} \gg 1$. The observed flux at high frequencies thus depends on the jet geometry. For wide jets, $a_{\rm jet} > 2/(p+1)$, the second term in the parenthesis of Equation (38) can be neglected. The flux above $\nu_{\rm peak,0}$ is therefore proportional to $F_\nu \propto B_0^{(p+1)/2}\nu^{-(p-1)/2}$. For narrower jets, $1/2 < a_{\rm jet} < 2/(p+1)$ and $\nu \ll \nu_{\rm max}$, the second term in the parenthesis of Equation (38) dominates, and one finds $F_\nu \propto B_0^{(p+1)/2}\nu^{1-1/a_{\rm jet}}$. The case of $a_{\rm jet} < 1/2$ is treated in Section 8.

5.2. Intermediate Magnetic Field: Gradual Change of the Spectral Slope at the X Band

If the magnetic field is in the range $B_{\rm cr,0} < B_0 < B_{\rm cr,1}$ then electrons at $\gamma_{\rm max}$ cool significantly at $t \gg t_0$, while electrons at the lower end of the energy distribution, $\gamma \gtrsim \gamma_{\rm min,}$ do not cool significantly. This introduces a break at $\nu_{\rm fast}$, given by Equation (26). We note that for $B_0 < B_{\rm cr,1}$, $\nu_{\rm fast} > \nu_{\rm peak,0}$. At the range $\nu_{\rm peak,0} < \nu < \nu_{\rm fast}$, the analysis carried out in Section 5.1 is valid. Hence, for wide jets $a_{\rm jet} > 2/(p+1)$, $F_\nu \propto \nu^{(p-1)/2}$. Similarly, at lower frequencies, $\nu < \nu_{\rm peak,0}$, $F_\nu \propto \nu^{1-1/a_{\rm jet}}$.

At higher frequencies, $\nu > \nu_{\rm fast}$, the spectrum is modified. Since the energetic electrons rapidly cool, emission at these high frequencies occurs only close to the jet base, where the magnetic field is constant. The flux at these frequencies can therefore be estimated by integrating the flux emitted from a jet segment, given by Equation (37), while keeping $B = B_0$ and $\nu_{\rm peak} = \nu_{\rm peak,0}$.

The length $\Delta x \equiv x_{\rm max}(\nu) - x_0$ during which electrons emit at frequency ν is related to the cooling rate of the energetic electrons. As this cooling rate is independent of the electrons initial energy, we can use the result derived in Section 4.2, Equation (34), to write $\Delta x = \gamma_j\beta_j c\delta t \approx 6\pi m_e c^2\gamma_j\beta_j/\sigma_T B_0^2(\gamma\beta)_{\rm max}$. As the electrons cool, the maximum emission frequency decays. Since the emission frequency $\nu \propto (\gamma\beta)^2$, emission at frequency ν can be obtained only from energetic electrons $(\gamma\beta)_{\rm max}(x)/(\gamma\beta)_{\rm min} = (\nu/\nu_{\rm peak,0})^{1/2}$. Using these results in Equation (37), one finds

$$F_\nu|_{\nu>\nu_{\rm fast}} = \frac{(m_e c^2)^2}{18\pi d^2 m_p c\Lambda}\frac{q_j\dot{M}_{\rm disk}}{B_0 q\theta_{\rm el,0}}\left(\frac{\nu}{\nu_{peak_0}}\right)^{-p/2}. \quad (39)$$

We therefore conclude that for intermediate magnetic field $B_{\rm cr,0} < B_0 < B_{\rm cr,1}$, the flux above $\nu_{\rm peak,0}$ changes from $F_\nu \propto \nu^{-(p-1)/2}$ below $\nu_{\rm fast}$, to $F_\nu \propto \nu^{-p/2}$ at higher frequencies. In reality, we do not expect a sharp cutoff at $\nu_{\rm fast}$, but a smooth connection (see Figure 5). This can be the source of the steep spectral slope observed in XTE J118+480 at the *X* band, and can affect our interpretation of the power-law index of the accelerated electrons. See further discussion in Section 9.

5.3. Strong Magnetic Field

By definition, if $B_0 > B_{\rm cr,1}$ then electrons at the peak of the Maxwellian, hence all the electrons above the peak rapidly cool by synchrotron emission close to the jet base. The results derived in the previous sections, Sections 4.2, 4.3, and 5.2, enable us to obtain the emission in the entire spectral range without the need for additional calculations.

Since $\nu_{\rm fast} < \nu_{\rm peak,0}$, the flux at $\nu_{\rm peak,0}$ is given by Equation (35), while the flux at higher frequencies drops as $F_\nu \propto \nu^{-p/2}$. At lower frequencies, $\nu_{\rm fast} < \nu < \nu_{\rm peak,0}$, the flux is $F_\nu \propto \nu^{-1/2}$. At even lower frequencies, $\nu < \nu_{\rm fast}$, the flux depends on the jet geometry, $F_\nu \propto \nu^{1-1/a_{\rm jet}}$. For an intermediate magnetic field, $B_0 < B_{\rm cr,2}$ the results of Section 4.2 show that at low frequencies $F_\nu \propto B_0$, while if the magnetic field is strong, $B_0 > B_{\rm cr,2}$, then the flux at low frequencies is suppressed by self-absorption, $F_\nu \propto B_0^{-8}$ (see Section 4.3).

Comparison of the flux for different values of the magnetic field is presented in Figure 5. As discussed above, regardless of the value of the magnetic field, the low-energy part of the spectrum, below $\nu_{\rm peak,0}$, is similar in this scenario and in the Maxwellian distribution scenario discussed in Section 4. We thus conclude that it is not possible to discriminate between these two initial distributions by observations at low energy, radio–IR bands. At higher frequencies, above $\nu_{\rm peak,0}$, the spectral slope gradually changes from $(p-1)/2$ for $B_0 < B_{\rm cr,0}$ to $p/2$ for $B_0 > B_{\rm cr,1}$. However, as is seen in the figure, this transition is gradual. We therefore expect an accurate measurement of the power-law index p to be difficult.

6. MAXWELLIAN DISTRIBUTION OF ELECTRONS WITH ADIABATIC ENERGY LOSSES

While in the previous sections we neglected adiabatic energy losses, in this section we consider these, in addition to the synchrotron losses. As a result, the electron temperature does not asymptote to a constant value, but continuously decreases as the electrons propagate along the jet (see Equation (13)). This introduces an additional break, $\nu_{\rm trans}$ (see Section 3.2, Equation (23)).

As we will show below, a major part of the analysis carried out in the previous sections holds here as well. This is due to the fact that in a strong magnetic field, the initial rapid cooling of the electrons close to the jet base, which determines the flux at high energies, is not affected by the inclusion of adiabatic losses (see discussion in Section 2.3). These only affect the late time decay of the electron temperature, hence the emission at low (radio) frequencies.

6.1. Weak Magnetic Field: Spectral Break at the Transition Frequency

If $B_0 < B_{\rm cr,1}$, then the initial rapid cooling is insignificant, and the electron temperature varies along the jet as $\theta_{\rm el} \propto x^{-2a_{\rm jet}/3}$ (see Equation (13)). The magnetic field also decays, and as a result, the peak frequency decays as $\nu_{\rm peak} \propto x^{-7a_{\rm jet}/3}$ and the break frequency decays as $\nu_{\rm thick} \propto x^{-2a_{\rm jet}/3}$ (see Section 3.2, Equation (21)). Assuming that at the jet base $\nu_{\rm peak,0} > \nu_{\rm thick,0}$, the difference in the decay laws introduces an additional break in the observed spectrum at frequency $\nu_{\rm trans}$ (Section 3.2, Equation (23)).

At the frequency range $\nu_{\rm trans} < \nu < \nu_{\rm peak,0}$, one can estimate the observed flux in a very similar way to the calculations done in Section 4.1, by integrating the emission from the different jet segments. The decay of the peak frequency implies that contribution to the flux at a given frequency $\nu < \nu_{\rm peak,0}$ is only from jet regions $x \leqslant x_{\rm max}$, where $x_{\rm max}/x_0 = (\nu/\nu_{\rm peak,0})^{-3/(7a_{\rm jet})}$. Integrating the emission from the jet segments $x_0 \leqslant x \leqslant x_{\rm max}$ while considering only the optically thin part of the spectrum (see Equation (11)) gives

$$F_\nu(\nu_{\rm trans} < \nu < \nu_{\rm peak,0}) \simeq \frac{2r_0^2 A_0}{9d^2}\frac{\theta_{\rm el_0}^3 q^3 B_0}{m_e c^2}\int_{x_0}^{x_{\rm max}}\left(\frac{x}{x_0}\right)^{-a_{\rm jet}} \times\left[\frac{3\nu}{4\nu_{\rm peak,0}}\left(\frac{x}{x_0}\right)^{7a_{\rm jet}/3}\right]^{1/3} dx = \left(\frac{3}{4}\right)^{1/3}\frac{2r_0^2}{9d^2}\frac{u_0 q^3 B_0 x_0}{(1-2a_{\rm jet}/9)m_e c^2 m_p c^2} \times\left(\frac{\nu}{\nu_{\rm peak,0}}\right)^{(3/7)(1-1/a_{\rm jet})}. \quad (40)$$

We therefore find that at the frequency range $\nu_{\rm trans} < \nu < \nu_{\rm peak,0}$, the flux depends on the jet geometry as $F_\nu \propto \nu^{(3/7)(1-1/a_{\rm jet})}$. This dependence is different than in the pure synchrotron case considered in Section 4.1, however we note that for conical jets ($a_{\rm jet} = 1$), still a flat spectrum is obtained. At frequencies higher than $\nu_{\rm peak,0}$, the flux decays exponentially for a Maxwellian distribution of electrons.

The main difference between this scenario and the pure synchrotron scenario discussed in Section 4.1 is the appearance of the transition frequency, $\nu_{\rm trans}$. This transition frequency is unavoidable, as it results from the different decay laws of $\nu_{\rm peak}$ and $\nu_{\rm thick}$ that take place as the electrons propagate along the jet. By definition, at frequencies $\nu < \nu_{\rm trans}$, the peak of the emission is in the optically thick part of the spectrum ($\nu_{\rm peak} < \nu_{\rm thick}$), and is thus obscured. The flux at low frequencies $\nu < \nu_{\rm trans}$ is therefore dominated by emission at $\nu_{\rm thick}$. This scenario is similar to the one discussed in Section 4.3. We showed there that for $\nu_{\rm peak} < \nu_{\rm thick}$, the evolution of $\nu_{\rm thick}$ is determined by solving the equation $[3\nu_{\rm thick}(x)/2\nu_{\rm peak}(x)]^{1/3} = (2/3)\log[\pi^2 r(x) A q^2 c/4\nu_{\rm thick}(x)]$. A rough estimate of the flux at low energies can be done by approximating the logarithm as constant, which enables us to write $\nu_{\rm thick} \propto \nu_{\rm peak} \propto x^{-7a_{\rm jet}/3}$. Since in this case of emission in the optically thick part of the spectrum, $dF_\nu \propto \nu^2 r\theta_{\rm el} dx \propto \nu^2 r^{1/3} dx$ (see Equation (10)), we conclude that $F_\nu(\nu < \nu_{\rm trans}) \propto \nu^{(13-3/a_{\rm jet})/7}$.

An example of the obtained spectrum is illustrated in Figure 6. The decomposition shows the evolution of the characteristic frequencies $\nu_{\rm thick}$ and $\nu_{\rm peak}$ along the jet. The faster decay of $\nu_{\rm peak}$ is clearly pronounced. We mark the transition frequency $\nu_{\rm trans}$. The different spectral regimes are easily identified in this plot.

6.2. Intermediate and Strong Magnetic Field

For higher values of the magnetic field $B_0 > B_{\rm cr,1}$, the electrons rapidly cool by synchrotron emission close to the jet base. Only after the initial rapid cooling, the electron temperature decay law asymptotes to $\theta_{\rm el} \propto x^{-2a_{\rm jet}/3}$. During the initial rapid decay the adiabatic energy losses are negligible (see Section 2.3, Equation (13)). This enables us to use the analysis carried out in Sections 4.2 and 4.3 in calculating the flux at high frequencies, which are dominated by emission during the initial rapid decay phase. On the other hand, the flux at low frequencies is governed by emission from electrons as they propagate along the jet. This enables us to use the analysis carried out for the case of weak magnetic field in Section 6.1 in calculating the flux at low frequencies.

For an intermediate magnetic field $B_{\rm cr,1} < B_0 < B_{\rm cr,2}$, similar analysis to the one carried out in Section 4.2 shows the existence of a break frequency at $\nu_{\rm fast}$, whose value is given in Equation (26). At the frequency range $\nu_{\rm fast} < \nu < \nu_{\rm peak,0}$, the flux decays as $F_\nu \propto \nu^{-1/2}$, and at higher frequencies, $\nu > \nu_{\rm peak,0}$, the flux decays exponentially.

The initial rapid cooling results in a shift of $\nu_{\rm trans}$ to higher frequency, given by Equation (24). As discussed in Section 3.3, for $B_0 < B_{\rm cr,2}$, $\nu_{\rm trans} < \nu_{\rm fast}$. Since below $\nu_{\rm fast}$ the analysis carried out in Section 6.1 holds, we conclude that at the range $\nu_{\rm trans} < \nu < \nu_{\rm fast}$, $F_\nu \propto \nu^{-(7/3)(1-1/a_{\rm jet})}$, while at lower frequencies $\nu < \nu_{\rm trans}$, $F_\nu(\nu < \nu_{\rm trans}) \propto \nu^{(13-3/a_{\rm jet})/7}$.

We thus conclude that for $B_{\rm cr,1} < B_0 < B_{\rm cr,2}$, the spectra below $\nu_{\rm peak,0}$ have three different regimes, separated by the two transition frequencies $\nu_{\rm trans}$ and $\nu_{\rm fast}$. In practice, however, we expect these transitions to be smooth, as is illustrated in Figure 7.

If the magnetic field is stronger, $B_0 > B_{\rm cr,2}$, then, by definition, emission below $\nu_{\rm fast}$ is in the optically thick part of the spectrum. In this case, $\nu_{\rm trans} = \nu_{\rm fast}$ (see discussion in Section 3.3). Thus, the spectrum below $\nu_{\rm peak,0}$ in this case is composed of only two segments: $F_\nu \propto \nu^{-1/2}$ for $\nu_{\rm fast} < \nu < \nu_{\rm peak,0}$ and $F_\nu \propto \nu^{(13-3/a_{\rm jet})/7}$ at lower frequencies. This is illustrated in Figure 8. We note that in this scenario, the requirement for a flat radio spectra ($F_\nu \propto \nu^0$ below $\nu_{\rm trans}$) cannot be fulfilled for $a_{\rm jet} > 1/2$.

7. POWER-LAW DISTRIBUTION OF ELECTRONS WITH ADIABATIC ENERGY LOSSES

When adiabatic energy losses are included, the electron power-law distribution above the Maxwellian affects not only the high-energy part of the spectrum ($\nu > \nu_{\rm peak,0}$), but also the very low energy part, $\nu < \nu_{\rm trans}$. This is due to the inclusion of $\nu_{\rm low}$, as discussed in Section 3.3.

The analysis of the spectra in this case is very similar to the analysis already done in the former sections. The observed

spectra are composed of several break frequencies, in accordance with the value of the magnetic field.

For a weak magnetic field, $B_0 < B_{\rm cr,0}$, the spectra are composed of four distinctive segments, separated by three break frequencies: $\nu_{\rm peak,0}$, $\nu_{\rm trans}$, and $\nu_{\rm low}$, given by Equations (4), (23), and (29). Above $\nu_{\rm peak,0}$ and below $\nu_{\rm max,0}$, the flux $F_\nu \propto \nu^{-(p-1)/2}$ is given by Equation (38) in Section 5.1. At the frequency range $\nu_{\rm trans} < \nu < \nu_{\rm peak,0}$, the results derived in Section 6.1 hold, and $F_\nu \propto \nu^{(3/7)(1-1/a_{\rm jet})}$.

At lower frequencies, $\nu_{\rm low} < \nu < \nu_{\rm trans}$, the flux can be calculated in the following way. We showed in Section 3.3 that the spectrum in this range is determined by emission from a power-law distribution of electrons at the break frequency $\nu_{\rm thick}$ which marks the transition from the optically thin to the optically thick part of the spectrum. In the optically thick part of the spectrum (Equation (10)), $dF_\nu \propto r^2(j_\nu/\tau\nu)dx \propto rB^{-1/2}\nu^{5/2}dx$, where j_ν and τ_ν are the emissivity and optical depth for power-law distribution of the emitting electrons (see Section 3.3). Using $\nu = \nu_{\rm thick}$, and the dependence of $\nu_{\rm thick}$ on the position along the jet as derived in Section 3.3, $\nu_{\rm thick} \propto r^{-A_1}$, one finds

$$dF_\nu \propto \nu^{5/2-\left(\frac{1}{A_1}\right)\left(\frac{3a_{\rm jet}+2}{2a_{\rm jet}}\right)}, \quad (41)$$

where $A_1(p) = (8+7p)/(3p+12)$ was derived in Section 3.3. The result in Equation (41) is identical to the result derived by Kaiser (2006); however, we note here that this result is valid only at the frequency range $\nu_{\rm low} < \nu < \nu_{\rm trans}$. Writing $F_\nu \propto \nu^\eta$ at this range, we find that for $p = 2$ (2.5), for $a_{\rm jet} = 1$, $\eta = 0.45\,(0.59)$, for $a_{\rm jet} = 3/4$, $\eta = 0.18\,(0.33)$, and for $a_{\rm jet} = 2/3$, $\eta = 0.05\,(0.20)$. One can thus conclude that for $a_{\rm jet} \lesssim 2/3$, a flat spectrum is expected at this range $\nu_{\rm low} < \nu < \nu_{\rm trans}$, similar to the conclusion in Kaiser (2006). At much lower frequencies $\nu < \nu_{\rm low}$ the discussion in Section 6.2 holds, and thus we can approximate $F_\nu \propto \nu^{(13-3/a_{\rm jet})/7}$. At high frequencies, $\nu > \nu_{\rm max,0}$, an exponential decay in the spectrum is expected.

From the discussion in Section 5, we find that the spectrum obtained for intermediate value of the magnetic field, $B_{\rm cr,0} < B_0 < B_{\rm cr,1}$, differs from the spectrum obtained for $B_0 < B_{\rm cr,1}$, by the inclusion of $\nu_{\rm fast}$ (Equation (26)). Since $\nu_{\rm fast} > \nu_{\rm peak,0}$, this inclusion only affects the energetic part of the spectrum: for $\nu > \nu_{\rm fast}$, $F_\nu \propto \nu^{-(p/2)}$, while the spectrum at lower frequencies is similar to the spectrum obtained in the weak magnetic field case derived above. For a magnetic field in this range, the values of $\nu_{\rm trans}$ and $\nu_{\rm low}$ are determined by Equations (24) and (30), respectively.

For higher values of the magnetic field, $B_{\rm cr,1} < B_0 < B_{\rm cr,2}$, $\nu_{\rm fast} < \nu_{\rm peak,0}$, and $\nu_{\rm low} = \nu_{\rm trans}$. The spectrum is thus separated into four distinctive regimes, which are different than those for the weak magnetic field derived above. For $\nu > \nu_{\rm peak,0}$, $F_\nu \propto \nu^{-(p/2)}$, and at lower frequencies $\nu_{\rm fast} < \nu < \nu_{{\rm peak},s}$, $F_\nu \propto \nu^{-1/2}$. At even lower frequencies, $\nu_{\rm trans} < \nu < \nu_{\rm fast}$, $F_\nu \propto \nu^{(3/7)(1-1/a_{\rm jet})}$, while at the low end of the spectra, $\nu < \nu_{\rm trans}$, $F_\nu \propto \nu^{(13-3/a_{\rm jet})/7}$.

For even higher values of the magnetic field, $B_0 > B_{\rm cr,2}$, $\nu_{\rm trans} = \nu_{\rm fast}$ are given by Equation (27). For this value of the magnetic field, there are only three distinctive spectral regimes below $\nu_{\rm max,0}$: $\nu < \nu_{\rm fast}$, $\nu_{\rm fast} < \nu < \nu_{\rm peak,0}$, and $\nu > \nu_{\rm peak,0}$. The flux in these regimes is similar to the flux in the equivalent regimes obtained for a weaker magnetic field.

Examples of the spectra obtained in this scenario are presented in Figures 9 and 10. In Figure 9 we present the dependence of the spectra on the strength of the magnetic field. We mark the transition frequencies. Note that for a strong magnetic field there is a degeneracy: e.g., as explained above, for $B_0 > B_{\rm cr,2}$, $\nu_{\rm low} = \nu_{\rm trans} = \nu_{\rm fast}$. In Figure 10 we give examples of the spectra obtained for the several possible jet geometries. Clearly, for low values of $a_{\rm jet}$, the flux at low frequencies, at the range $\nu_{\rm low} < \nu < \nu_{\rm trans}$, increases (this holds only as long as $a_{\rm jet} > 1/2$), while the flux at high frequencies, $\nu > \nu_{\rm peak,0}$, is unaffected. The theoretical approximation in Equation (41) predicts that for a power-law index $p = 2.5$ as is used in the plots, flat spectra are obtained for $a_{\rm jet} = 0.56$. The numerical result is in very good agreement with this prediction.

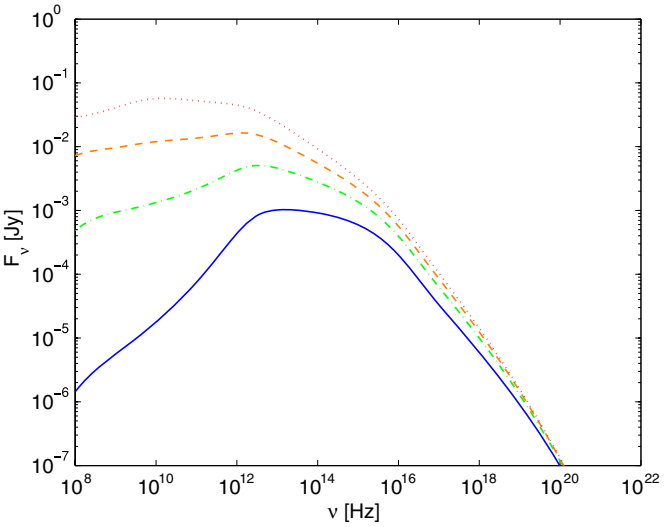

Figure 10. Examples of spectra obtained from an initial power-law distribution of electrons with power-law index $p = 2.5$ when adiabatic energy losses are included, for different jet geometries. A conical jet $a_{\rm jet} = 1.0$ (solid, blue), $a_{\rm jet} = 2/3$ (dash-dotted, green), $a_{\rm jet} = 0.56$ (dash-dash, orange), and $a_{\rm jet} = 0.5$ (dotted, red). The magnetic field is taken as $B_0 = 3 \times 10^3$ G $< B_{\rm cr,1}$, and all the other parameters are the same as in Figure 2. For $a_{\rm jet} = 0.56$, the analytical result in Equation (41) predicts a flat spectrum $F_\nu \propto \nu^0$ at the range $\nu_{\rm low} < \nu < \nu_{\rm trans}$. The numerical result shows very good agreement with this prediction.

(A color version of this figure is available in the online journal.)

8. NARROW JETS

As discussed in Section 2.3, for narrow jets $a_{\rm jet} < 1/2$, the electrons lose their momentum asymptotically as $\gamma\beta \propto x^{2a_{\rm jet}-1}$. This asymptotic decay law is independent of the inclusion of adiabatic energy losses. Therefore, the analysis is similar in both scenarios. Moreover, due to the continuous electron energy loss along the jet, the analysis is essentially similar to the analysis carried out in Sections 6 and 7 where adiabatic energy losses were included. We give here a brief description of the spectrum obtained in this case. As we will show below, we find it impossible to obtain flat radio spectra, as suggested by many observations. We thus find this scenario less likely.

The high-energy part of the spectra, at $\nu > \min(\nu_{\rm peak,0}, \nu_{\rm fast})$, is determined by electrons close to the jet base, and is therefore unaffected by the jet geometry. The analysis in the previous sections is thus valid in this case as well.

The difference in the flux emitted in this scenario and the scenarios discussed above is thus expected at lower frequencies, $\nu < \min(\nu_{\rm fast}, \nu_{\rm peak,0})$. The flux at $\nu_{\rm trans} < \nu$ can be calculated from the decay law of the electron energy. At this frequency range, the peak of the synchrotron emission from any jet segment is in the optically thin part of the spectrum. As a result, one can write $\nu_{\rm peak} \propto (\gamma\beta)^2 B \propto x^{3a_{\rm jet}-2}$, and using Equation (11), $F_\nu \propto r^2 n(r) B dx \propto x^{1-a_{\rm jet}}$. One therefore concludes that at this

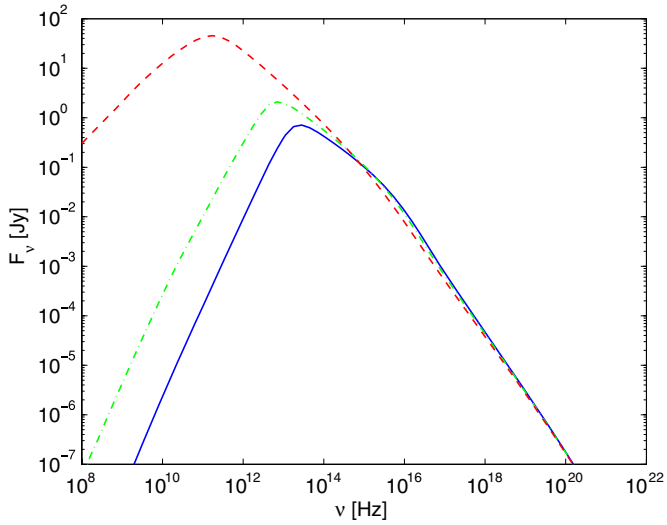

Figure 11. Examples of spectra from a power-law distribution of electrons with index $p = 2.5$ for different jet geometries in narrow jets. Shown are $a_{\rm jet} = 0.1$ (solid, blue), $a_{\rm jet} = 0.2$ (dash-dotted, green), $a_{\rm jet} = 1/3$ (dash-dash, red). The magnetic field is taken as $B_0 = 3 \times 10^3$ G $< B_{\rm cr,1}$, and all the other parameters are the same as in Figure 2. The transition frequency $\nu_{\rm trans}$ is clearly seen. In no case can a flat radio spectrum be obtained (see the text for details).

(A color version of this figure is available in the online journal.)

frequency range $F_\nu \propto \nu^{\eta_1}$, with $\eta_1 = (1 - a_{\rm jet})/(3a_{\rm jet} - 2)$. For $a_{\rm jet} = 0$, we find $\eta_1 = -1/2$ while for $a_{\rm jet} = 1/2$, $\eta_1 = -1$.

If the electrons have a Maxwellian distribution, then at lower frequencies, $\nu < \nu_{\rm trans}$, the peak of the emitted spectrum is obscured. Using Equation (10), one finds $dF_\nu \propto \nu^2 r\theta_{\rm el} dx \propto x^{9a_{\rm jet}-4}$. We have used here similar arguments to the ones used in Section 6.1, which enables us to estimate the x-dependence of $\nu_{\rm thick}$ as similar to that of $\nu_{\rm peak}$ at low frequencies. We therefore conclude that at this frequency range, $F_\nu \propto \nu^{\eta_2}$, with $\eta_2 = (9a_{\rm jet} - 4)/(3a_{\rm jet} - 2)$. For $a_{\rm jet} = 0$, $\eta_2 = 2$ while for $a_{\rm jet} = 1/3$, $\eta_2 = 1$. For a somewhat wider jet, $a_{\rm jet} = 4/9$, $\eta_2 = 0$, and a flat spectrum is obtained. However, as pointed out in Section 3.2, for $a_{\rm jet} \approx 0.45$, the transition frequency is very low, $\nu_{\rm trans} \approx 10^6$ Hz. As a result, the flat part of the spectra occurs at frequencies well below current observation capabilities.

If the electrons have a power-law distribution above $\gamma_{\rm min}$, then the observed spectrum below $\nu_{\rm trans}$ shows an additional break, at $\nu_{\rm low}$. Similar to the discussion in Section 7, for $\nu < \nu_{\rm low}$, $F_\nu \propto \nu^{\eta_2}$. The flux in the intermediate range, $\nu_{\rm low} < \nu < \nu_{\rm trans}$, is calculated as follows. An analysis similar to the one carried out in Section 3.3 shows that in this case, when writing the electron distribution as $n_{\rm el}(\gamma)d\gamma = k(x)\gamma^{-p}d\gamma$, the proportionality constant evolves as $k(x) \propto x^{1-4a_{\rm jet}+p(2a_{\rm jet}-1)}$, resulting in $\nu_{\rm thick} \propto x^{[a_{\rm jet}(3p-8)+2(1-p)]/(p+4)}$. For $p = 2$ this results in $\nu_{\rm thick} \propto x^{-(1+a_{\rm jet})/3}$, while for $p = 2.5$ one obtains $\nu_{\rm thick} \propto x^{-(6+a_{\rm jet})/13}$. Using $dF_\nu \propto rB^{-1/2}\nu^{5/2}dx$, one finds that for $p = 2$, $dF_\nu \propto \nu^{-(1+4a_{\rm jet})/(2+2a_{\rm jet})}$, while for $p = 2.5$, $dF_\nu \propto \nu^{(4-34a_{\rm jet})/(12+2a_{\rm jet})}$. We thus conclude that for $p = 2$, the flux varies from $F_\nu \propto \nu^{-1/2}$ for $a_{\rm jet} = 0$, to $F_\nu \propto \nu^{-1}$ for $a_{\rm jet} = 1/2$. For $p = 2.5$, a flat spectrum can actually be obtained at this range $\nu_{\rm low} < \nu < \nu_{\rm trans}$, but only for very narrow jets, $a_{\rm jet} = 0.1$. For such a narrow jet, the analysis carried out in Sections 3.2 and Section 3.3 shows that $\nu_{\rm low} \lesssim \nu_{\rm trans}$, and thus the flat spectrum is limited to a very narrow band, and in practice does not exist.

Examples of the spectra for the various jet geometries are presented in Figure 11. The transition frequency $\nu_{\rm trans}$ is clearly seen to evolve to lower frequencies when $a_{\rm jet}$ increases, as is predicted in Section 3.2.

9. SUMMARY AND DISCUSSION

In this paper, we have extensively studied a model for synchrotron emission from jets in BHXRBs. Our basic assumption is that the electrons are accelerated once at the base of the jet, and lose their energy by synchrotron emission and possible adiabatic energy losses, as they propagate along the jet. As the details of the acceleration process are not understood from first principles, we considered two scenarios which have strong theoretical and observational motivations: a Maxwellian distribution of energetic electrons, and a power-law distribution above the low-energy Maxwellian, at the energy range $\gamma_{\rm min} < \gamma < \gamma_{\rm max}$, with an exponential decay at higher energies. The inclusion of a low-energy cutoff to the accelerated electron energy distribution directly implies a characteristic break frequency in the observed spectra, at $\nu = \nu_{\rm peak,0}$ (see Equation (4)). This break frequency adds to the break frequency $\nu_{\rm thick}$ which marks the transition from the optically thin to the optically thick emission.

We assume that the magnetic field decays along the jet in accordance with Poynting-flux conservation, $B(r) \propto r^{-1}$. We showed in Section 2.3 that the electron cooling along the jet has an analytical description (see Equations (13) and (14)). These equations hold the key to the rest of the analysis. By studying the cooling rates, we found that in a strong magnetic field, the cooling can be separated into two distinctive regimes: an initial rapid cooling that takes place close to the jet base, during which the electrons emit at high frequencies (UV, X-, and γ-rays), and a secondary long phase in which the electron cooling rate asymptotes. For wide jets, $a_{\rm jet} > 1/2$, when only synchrotron emission is considered, the electrons energy becomes time (and x) independent, $\gamma \propto x^0$; when adiabatic energy losses are considered, then $\gamma \propto x^{-2a_{\rm jet}/3}$. For narrow jets, both scenarios result in a similar asymptotic decay law, $\gamma \propto x^{2a_{\rm jet}-1}$.

These results enabled us to define in Section 3.1 critical values of the magnetic field, and in Sections 3.2 and 3.3, five transition frequencies in the observed spectra. We then analyzed the resulting spectra for the various assumptions on the accelerated electrons' spectra. A Maxwellian distribution was considered in Sections 4 and 6, and power-law spectra were considered in Sections 5 and 7. We further studied the effect of inclusion of adiabatic energy losses in Sections 6 and 7, and the unique scenario of narrow jets, $a_{\rm jet} < 1/2$, in Section 8.

While the variety of spectra that can be obtained in such a simplistic model is found to be very large, we can point to some general properties of the spectra that we find of high importance.

1. Flat radio spectra, as is seen in many objects, can be obtained if only synchrotron emission is considered, for conical jets (see Sections 4 and 5, Figures 2–5), regardless of the value of the magnetic field. This scenario is similar to the original model of Blandford & Königl (1979), although there is a different physical origin for the flat spectrum: here the flat spectrum results from a decay of the peak of the emission frequency $\nu_{\rm peak}$ along the jet, while in Blandford & Königl (1979) model, the evolution of $\nu_{\rm thick}$ was considered. As we showed in Section 3.2, neglecting adiabatic energy losses, both frequencies evolve in a similar way. We further showed that when adiabatic energy losses are included, a flat spectrum can be obtained for conical jets only above $\nu_{\rm trans}$, whose value is given in Equation (23) (see Sections 6

and 7, Figures 6–9). At lower frequencies, a flat spectrum can be obtained only when a series of conditions are met: the electrons are power-law distributed, the jet has a specific geometry (see Section 7, Equation (41) and Figure 10), and the magnetic field is limited. In this case, a flat spectrum is obtained only at the range $\nu_{\rm low} < \nu < \nu_{\rm trans}$. For narrow jets, we showed in Section 8 that a flat radio spectra cannot be achieved (see Figure 11).

2. We showed that the flux at the radio wavelengths depends on the value of the magnetic field in a nontrivial way: for magnetic field at the jet base $B_0 < B_{\rm cr,2}$, the flux increases with the increase in the magnetic field (see Section 4.1). However, for stronger magnetic field, $B_0 > B_{\rm cr,2}$ a further increase in the magnetic field at the jet base leads to a rapid decrease of the observed radio flux, due to an increase in the optical depth (see Section 4.3). This is not accompanied by a similar change in the flux at higher frequencies, $\nu > \nu_{\rm fast}$: the flux at high frequencies asymptotes to a constant value in a strong magnetic field, $B > B_{\rm cr,1}$. We therefore find a natural mechanism that can lead to a variation in the ratio of the radio to X-ray fluxes, by a simple change in the value of the magnetic field. We further investigate the consequences of this idea in a forthcoming paper (P. Casella & A. Pe'er 2009, in preparation). These results imply that the strongest radio emission occurs for $B_0 \approx B_{\rm cr,2}$, or about three orders of magnitude below equipartition value. While the origin of the magnetic field in jets is not understood from first principles, we believe that this value could be used as a guideline for models of magnetic field production near the jet base.
3. We showed that for intermediate values of the magnetic field $B_0 > B_{\rm cr,0}$, the flux at X-ray wavelength gradually changes from $(p-1)/2$ at low energies to $p/2$ at higher energies, due to the rapid cooling of the most energetic electrons (see Section 5.2). For an even higher value of the magnetic field, $B_0 > B_{\rm cr,1}$, we found that at the range $\nu_{\rm fast} < \nu < \nu_{\rm peak,0}$, which is typically in the optical-to-X-ray band, the flux decays as $F_\nu \propto \nu^{-1/2}$ (see Section 4.2). This decay law occurs close to the jet base, and is therefore independent of the jet geometry.
   This gradual transition of the flux implies that every attempt to determine the power-law index p of the accelerated electrons by fitting X-ray data should be done with great care. The result $F_\nu \propto \nu^{-1/2}$ above $\nu_{\rm fast}$ is very robust, as it is independent of the initial distribution of the electrons, or of the exact value of the magnetic field. It can easily be misinterpreted as due to synchrotron emission from a power-law distribution of electrons, whose cooling is insignificant. Under this interpretation, one would come to the wrong conclusion that the power-law index p of the accelerated electrons is $p = 2$. Similarly, at higher frequencies, the gradual change of the spectral slope from $(p-1)/2$ to $p/2$ as predicted here, if fitted using a single power law over a limited band, can lead to a wrong conclusion about the value of the power-law index p. This may be the source of the discrepancy between measurements of the index p in BHXRBs and in other objects, as discussed in Section 1.
4. We obtained high radio flux, ~ 10 mJy, for parameters that characterize emission from XTE J1118+480, in models of wide jets. This is similar flux to that observed in this object (Hynes et al. 2000). While we did not aim to fit data in this manuscript, we find these results encouraging. We further point out that the terms "wide" and "narrow" jets used here can be somewhat misleading, since they refer only to the confinement of the jet. A "wide" jet as defined here can be geometrically very narrow.

Our model is of course far from being able to describe the full physical processes that are expected to occur inside the jets. Several radiative processes, like Compton scattering, pair production, or the full effect of synchrotron self-absorption on the electron energy distribution, are not considered here (see the Appendix). However, these phenomena have only minor effects on the resulting spectra under the conditions assumed here (see, e.g., Kaiser 2006). Moreover, we did not consider in this work the possible contribution of internal energy dissipations (e.g., internal shocks) that can lead to multiple acceleration episodes of electrons as they propagate along the jet.

Multiple acceleration episodes of electrons along the jet result in a complicated spectra, whose details depend on the details of the acceleration processes (e.g., position, fraction of particles that are being accelerated, strength of the magnetic field at the acceleration sites, etc.). The spectra obtained in this work can therefore be viewed as a basic ingredient of the spectra that result from such multiple accelerations: a spectrum in the more complicated case can be obtained by a composition of the spectra presented here. In this manuscript, we focused on the spectra that result from a single acceleration episode, in order to demonstrate the key physical processes that occur in the plasma. While our numerical model can very easily be generalized to include multiple acceleration episodes, due to the expected complexity of the spectra in this case, we leave this for a future work. We do stress though that any model that considers particle acceleration to high energies should treat this phenomenon separately than synchrotron and adiabatic cooling, since these phenomena have different physical origins.

One of the key uncertainties in models of emission from jets, when internal dissipation of energy takes place, involves the origin of the magnetic field. Here, we assumed that the magnetic field originates at the core, and evolves according to Poynting-flux conservation law. However, an alternative scenario may be that the magnetic field is produced by the internal shock waves. In such a scenario, the magnetic field would evolve in a different way, thus some of the results derived here would not hold. Such a scenario was considered by Kaiser (2006), where, however, a low-energy cutoff in the accelerated electron distribution was not included, which has a strong influence on the obtained results. A full treatment of the spectral dependence on the origin of the magnetic field is left for future work.

We discussed in this work emission from jets in the low/hard state of BHXRB candidates, since in this state there is good evidence for the existence of jets. However, the physics of emission from jets in other sources, like AGNs are most probably very similar. We thus expect that many of the results found here should be relevant for jets in other astronomical sources as well.

We would like to thank Dipankar Maitra and Sera Markoff for careful reading of the manuscript and for many useful comments and discussions. We would further like to thank Ed van den Heuvel, Rob Fender, Ralph A.M.J. Wijers, Peter Mészáros, Bing Zhang, Mario Livio, and Martin J. Rees for useful discussions. A.P. is supported by the Riccardo Giacconi Fellowship award of the Space Telescope Science Institute. This work was partially supported by the Netherlands Organization for Scientific Research (NWO).

APPENDIX

NUMERICAL CODE

The numerical code is based on the code constructed by Pe'er & Waxman (2005) in the study of emission from GRBs. The particles are assumed to be accelerated at the base of the jet. A fraction $0 \leqslant \epsilon_{\rm pl} \leqslant 1$ is assumed to have a power-law distribution between $\gamma_{\rm min}$ and $\gamma_{\rm max}$, while $1 - \epsilon_{\rm pl}$ of the particles have a low-energy Maxwellian tail below $\gamma_{\rm min}$. The particles energy distribution is discretized in momentum space ($\gamma\beta$) in order to obtain accurate calculations when the electron cooling is significant. The code gets as an input the parameters of the flow (see Section 2.1), and calculates the number and energy densities of the electrons at the jet base.

The code divides the jet into segments, and evolves the magnetic field at each segment, in accordance with $B(x) \propto x^{-a_{\rm jet}}$. Both B_0 and $a_{\rm jet}$ are considered free parameters. Given the strength of the magnetic field, the code calculates the rate of electron cooling as the electrons propagate through each segment (Equation (12)). In parallel, the emitted flux from each segment (Equation (9)) is calculated self-consistently by solving the radiative transfer equation. When calculating the emissivity, the full cyclo-synchrotron spectra from each momentum bin are calculated (Mahadevan et al. 1996; Pe'er & Waxman 2005). Since the magnetic field varies along the jet, the emissivity is calculated for a reference value of the magnetic field and is tabulated. As the magnetic field evolves along the jet, the characteristic frequencies decay; however, using the scaling law for the emitted frequencies, $\nu = \nu_0 \times (B/B_0)$, and emitted power, $P(\nu) = P[\nu_0 \times (B/B_0)](B/B_0)$, the full emissivity at any given jet segment is readily obtained by interpolating from the saved values. Given the emissivity at each segment, the self-absorption coefficient is calculated by solving the integro-differential equation (Rybicki & Lightman 1979, Equation (6.50)), which is correct for a general distribution of electrons. Calculation of the optical depth follows the assumption that the line of sight is perpendicular to the jet axis.

When adiabatic energy losses are considered, Equation (2), which is accurate for any value of the electron momentum, is used. The discrete electron momentum levels are kept constant. Therefore, calculation of the electron cooling is done in two steps. The first step is to obtain their new momentum, by solving Equation (2). At a second step, the new electron distribution is fitted to the original, discrete cells. We use a second-order fit in logarithmic space of both the electrons' number and their momentum, which is proven to conserve both number and energy density.

In this version of the code we do not assume any further interactions between the photons and the electrons (e.g., Compton scattering, increase in the electrons energy due to synchrotron self-absorption, pair production). We therefore found that a simple first-order integration scheme is sufficient in calculating the evolution of the electrons' energy distribution.

REFERENCES

Amato, E., & Blasi, P. 2006, MNRAS, 371, 1251
Axford, W. I. 1994, ApJS, 90, 937
Blandford, R. D., & Eichler, D. 1987, Phys. Rep., 154, 1
Blandford, R. D., & Königl, A. 1979, ApJ, 232, 34
Blandford, R. D., & Rees, M. J. 1974, MNRAS, 169, 395
Bosch-Ramon, V., Romero, G. E., & Paredes, J. M. 2006, A&A, 447, 263
Celotti, A., & Ghisellini, G. 2008, MNRAS, 385, 283
Chaty, S., et al. 2003, MNRAS, 346, 689
Coppi, P. S. 1999, in ASP Conf. Ser. 161, High Energy Processes in Accreting Black Holes, ed. J. Poutanen & R. Svensson (San Francisco, CA: ASP), 375
Corbel, S., Nowak, M. A., Fender, R. P., Tzioumis, A. K., & Markoff, S. 2003, A&A, 400, 1007
Corbel, S., et al. 2000, A&A, 359, 251
Esin, A. A., et al. 1997, ApJ, 489, 865
Esin, A. A., et al. 2001, ApJ, 555, 483
Falcke, H., & Biermann, P. L. 1995, A&A, 293, 665
Fender, R. 2001, MNRAS, 322, 31
Fender, R. 2006, in Compact Stellar X-Ray Sources, ed. W. H. G. Lewin & M. M. van der Klis (Cambridge: Cambridge Univ. Press), 381
Fender, R., et al. 1999, MNRAS, 304, 865
Freedman, D. L., & Waxman, E. 2001, ApJ, 547, 922
Galama, T., Wijers, R. A. M. J., Bremer, M., Groot, P. J., Strom, R. G., Kouveliotou, C., & van Paradijs, J. 1998, ApJ, 500, L97
Gallo, E., Fender, R. P., & Pooley, G. G. 2003, MNRAS, 344, 60
Gallo, E., et al. 2007, ApJ, 670, 600
Georganopoulos, M., & Marscher, A. P. 1998, ApJ, 506, 621
Giannios, D., & Spruit, H. 2006, A&A, 450, 887
Hannikainen, D. C., Hunstead, R. W., Campbell-Wilson, D., & Sood, R. K. 1998, A&A, 337, 460
Hjellming, R. M., & Johnston, K. J. 1988, ApJ, 328, 600
Hynes, R. I., et al. 2000, ApJ, 539, L37
Jamil, O., Fender, R. P., & Kaiser, C. 2008, in Proceedings of Science, VII Microquasar Workshop: Microquasars and Beyond, in press (arXiv:0811.3320)
Jones, T. W., & Hardee, P. E. 1979, ApJ, 228, 268
Kaiser, C. R. 2006, MNRAS, 367, 1083
Kaiser, C. R., Sunyaev, R., & Spruit, H. C. 2000, A&A, 356, 975
Kalemci, E., et al. 2005, ApJ, 622, 508
Komissarov, S. S., Barkov, M. V., Vlahakis, N., & Königl, A. 2007, MNRAS, 380, 51
Lazendic, J. S., Slane, P. O., Gaensler, B. M., Reynolds, S. P., Plucinsky, P. P., & Hughes, J. P. 2004, ApJ, 602, 271
Liang, E. P. 1998, Phys. Rep., 302, 67
Longair, M. S. 1994, High Energy Astrophysics (Cambridge: Cambridge Univ. Press)
Mahadevan, R., Narayan, R., & Yi, I. 1996, ApJ, 465, 327
Markoff, S., Falcke, H., & Fender, R. 2001, A&A, 372, L25
Markoff, S., Nowak, M. A., & Wilms, J. 2005, ApJ, 635, 1203
Markoff, S., et al. 2003, A&A, 397, 645
Mc Clintock, J. E., & Remillard, R. E. 2006, in Compact Stellar X-Ray Sources, ed. W. H. G. Lewin & M. M. van der Klis (Cambridge: Cambridge Univ. Press), 157
Migliari, S., et al. 2007, ApJ, 670, 610
Mirabel, I. F., & Rodriguez, L. F. 1999, ARA&A, 37, 409
Paredes, J. M., Bosch-Ramon, V., & Romero, G. E. 2006, A&A, 451, 259
Pe'er, A., & Waxman, E. 2004, ApJ, 613, 448
Pe'er, A., & Waxman, E. 2005, ApJ, 628, 857
Poutanen, J. 1998, in Theory of Black Hole Accretion Disks, ed. M. A. Abramowicz, G. Bjornsson, & J. E. Pringle (Cambridge: Cambridge Univ. Press), 100
Reynolds, S. P. 1982, ApJ, 256, 13
Rybicki, G. B., & Lightman, A. P. 1979, Radiative Processes in Astrophysics (New York: Wiley)
Spada, M., Ghisellini, G., Lazzati, D., & Celotti, A. 2001, MNRAS, 325, 1559
Spitkovski, A. 2008, ApJ, 682, L5
Titarchuk, L. 1994, ApJ, 434, 570
Ustyugova, G. V., Lovelace, R. V. E., Romanova, M. M., Li, H., & Colgate, S. A. 2000, ApJ, 541, L21
Vrtilek, S. D. 2008, in AIP Conf. Ser. 1010, A Population Explosion: The Nature & Evolution of X-ray Binaries in Diverse Environments, ed. R. M. Bandyopadhyay (Melville, NY: AIP), 18
Wijers, R. A. M. J., & Galama, T. J. 1999, ApJ, 523, 177
Zdziarski, A. A. 2000, in IAU Symp. 195, Highly Energetic Physical Processes and Mechanisms for Emission from Astrophysical Plasmas, ed. P. C. H. Martens, S. Tsuruta, & M. A. Weber (San Fransisco, CA: ASP), 153